POLITECNICO DI TORINO
Repository ISTITUZIONALE

Planning interventions in a controlled pandemic: the COVID-19 case

Terms of use:

(Article begins on next page)

15 January 2025

Planning interventions in a controlled pandemic: the COVID-19 case

Franco Galante, Chiara Ravazzi, *Member, IEEE*, Michele Garetto, *Member, IEEE*, Emilio Leonardi, *Senior Member, IEEE*

Abstract—Restrictions on social and economic activities, as well as vaccinations, have been a key intervention in containing the COVID-19 epidemic. Our work focuses on better understanding the options available to policymakers under the conditions and uncertainties created by the onset of a new pandemic. More precisely, we focus on two control strategies. The first aims to control the rate of new infections to prevent congestion of the health care system. The latter directly controls hospitalizations and intensive care units (ICUs) occupation. By a first-order analysis, we show that, on the one hand, due to the difficulty in contact tracing and the lack of accurate information, controlling the transmission rate may be difficult, leading to instability. On the other hand, although hospitalizations and ICUs are easily accessible and less noisy than the rate of new infections, a delay is introduced in the control loop, which may endanger system stability. Our framework allows assessing the impact on economic and social costs of the above strategies in a scenario enriched by: i) population heterogeneity in terms of mortality rate and risk exposure, ii) closed-loop control of the epidemiological curve, and iii) progressive vaccination of individu

Index Terms—Control strategies analysis, stability analysis, delay differential equations, population heterogeneity modeling, closed-loop control system.

I. INTRODUCTION

Throughout the recent COVID-19 pandemic, governments worldwide faced the challenge of developing effective strategies to contain the virus while minimizing its economic and societal impact. As new waves of infection emerge, swift implementation of regulations becomes imperative to curtail human mobility and activities that facilitate virus transmission. From the pandemic onset, it was evident [1] that governments would face a delicate balance between reducing COVID-19 fatalities and mitigating the economic fallout caused by the spread of the virus. While individuals prioritize preserving life, governments must take action to manage the inevitable economic downturn.

Once the epidemiological curve starts to decline, policymakers in democratic nations often face pressure from various stakeholders to ease restrictions and resume suspended activities. Striking an equilibrium becomes desirable to ensure

F. Galante and Emilio Leonardi are with the Politecnico di Torino, Department of Electronics and Telecommunication (DET), Corso Duca Degli Abruzzi, 10129, Italy. E-mail: franco.galante@polito.it, E-mail: emilio.leonardi@polito.it.

C. Ravazzi is with the Institute of Electronics, Computer and Telecommunication Engineering, National Research Council of Italy (CNR-IEIIT), c/o Politecnico di Torino, Corso Duca Degli Abruzzi, 10129, Italy. E-mail: chiara.ravazzi@ieiit.cnr.it

M. Garetto is with the University of Turin, Computer Science Department, Corso Svizzera 185, 10149 Torino, Italy. E-mail: michele.garetto@unito.it

E. Leonardi is with the Politecnico di Torino, Department of Electronics and Telecommunication (DET) and research associate at National Research Council of Italy (CNR-IEIIT). E-mail: emilio.leonardi@polito.it.

both economic and social well-being, where the spread of the virus is effectively controlled with minimal limitations, as emphasized in [2].

About a year into the COVID-19 pandemic, several vaccines against the virus started to become available. However, the availability of these vaccines was initially limited, and their effectiveness in preventing infection not yet fully understood. In light of these uncertainties, developing strategies to prioritize vaccine distribution became challenging. The interested reader can refer to [3] for insights and analysis on the complexities of developing effective vaccine prioritization strategies in such uncertain times.

In this study, our objective is to enhance our comprehension of the choices that policymakers have at their disposal during conditions of a pandemic emergency. We aim to explore in-depth different strategies, measures and approaches that policymakers can consider and implement to effectively respond to the challenges posed by a pandemic aiming at safeguarding public health, minimizing the impact on society, and ensuring the well-being of individuals.

A. Modeling epidemic spread

The introduction of the SIR model in [4] marked a significant milestone in utilizing mathematical models to understand disease dynamics and forecast the spread of epidemics. SIR-like models divide the population into compartments based on disease status, defining transitions among them. We refer to the Supplemental Material [5] for an overview. Many of these models assume homogeneous populations, disregarding the intrinsic heterogeneity of society. The authors of [6] provide a more accurate description, where they introduce age-specific contact patterns.

Historically, the focus of studies in the field of epidemiology has primarily been on understanding the phenomenological aspects of epidemics. These studies aimed to assess the accuracy of different models in predicting the evolution of epidemics and identifying easily interpretable parameters that capture the qualitative behavior of infectious diseases. One such parameter of significant interest has been the *basic reproduction number*, which characterizes the conditions under which an infection outbreak can occur. There is a growing recognition of the need to proactively design *simple* and effective control measures to combat and mitigate the spread of infectious diseases in the possibility of future pandemics. We refer the readers to [7], which offers an overview of various mathematical models for epidemic processes, encompassing traditional group models with no assumed graph structures, network-based models, stability analysis, parameter estimation methods, and simulation models.

B. Control via non-pharmaceutical interventions

In this paper, we assume a central planner perspective, where the government can impose control measures on the population for the overall benefit of public health. Several papers published in the 1970s, such as [8]–[12], focused on studying optimal control problems in the context of the classical SIR model. Building upon these foundations, subsequent works like [13] and [14] expanded on the research and extended the models. These studies specifically addressed the challenge of minimizing the size of an epidemic outbreak and the cost of interventions. The control mechanisms explored in these models included regulating social distancing levels and implementing measures like isolation. These control strategies were also subject to rate constraints, ensuring the rate remained below a specified threshold. Papers on optimal control problems [15], [16] consider the minimization of a composite function taking into account the epidemic cost, related to the size of the outbreak or number of deaths, and the economic cost. The control perspective has been widely embraced in recent literature regarding the COVID-19 pandemic. Consequently, there has been considerable discussion about the effects of lockdown measures on healthcare, society, and the economy. The problem of minimizing the cost of a lockdown under the only constraint of maintaining the infection below a certain threshold to cope with ICU congestion problems is also considered in [17].

C. Control via vaccination

The paper [18] focuses on the optimal control of vaccination dynamics during an influenza epidemic. It provides insights into the design of vaccination strategies to effectively control the spread of the disease, considering factors such as limited vaccine supply and variations in transmission and severity across different groups. In [19], optimal vaccination and treatment strategies are studied in a multi-group epidemic model. The analysis explores the trade-offs between vaccination coverage and treatment allocation to maximize overall disease control, considering the interactions between different population groups. Finally, [20] explores the optimal timing and allocation of vaccinations based on age groups to maximize the effectiveness of the vaccination campaign and minimize the spread of infectious diseases. The research conducted in [21] and [22] contributes to the field by addressing the challenge of resource allocation for vaccination efforts in the context of epidemic control. By utilizing optimization techniques, these studies provide insights into the most effective strategies for targeting specific nodes in a contact network or groups within a population, considering both the budgetary constraints and the dynamics of disease transmission.

D. Main contribution

This paper investigates a novel class of compartmental models that draw inspiration from the features of the COVID-19 epidemic. We enhance previous models by incorporating: i) variability in mortality rate and risk exposure among different population segments, ii) closed-loop control mechanisms to regulate the epidemiological curve, and iii) progressive vaccination campaigns. More precisely, differently from previous works on the subject (see [23], [24], [25], [26], [27], [28], [29]), our modeling framework explicitly represents the heterogeneity of risk exposure across population segments.

Our study takes a different perspective than the optimal control approach. We deliberately examine *simple* control strategies to provide practical insights and guidelines for decision-makers who may not have access to sophisticated optimization techniques or detailed knowledge of the underlying epidemic mathematical laws (e.g., parameters).

Optimal control approaches in epidemiology have certain drawbacks worth mentioning. These approaches often lack closed-form analytical solutions, requiring numerical methods for their implementation [30], [31]. While numerical solutions can provide valuable insights, they can be challenging to interpret and translate into practical control measures. This lack of interpretability hampers the ability to univocally understand the implications and consequences of the obtained optimal control strategies. Another drawback is that optimal control solutions may strongly depend on parameters, leading to abrupt changes in the optimal interventions. These "phase transitions" can make implementing and managing the control measures in practice difficult. Minor changes in the parameters or system conditions may result in significant shifts in the optimal strategies. Furthermore, optimal control approaches often rely on detailed and precise knowledge of the system dynamics, including accurate parameter values and functional forms of the underlying equations. In real-world scenarios, such detailed information may be unavailable or subject to significant uncertainties. In the same spirit as [32], we will mainly focus on two control feedback strategies based on controlling the rate of new infections or maintaining the occupation of healthcare facilities below a given level, and we evaluate the economic cost of non-pharmaceutical interventions and the social cost in terms of number of deaths. For the sake of simplicity and analytical tractability, we consider an "ideal" scenario in which the system operates near the equilibrium point, where the effective reproduction number equals one (we provide local stability results). This regimen appears to be a desirable condition whereby the number of infected individuals, and thus those requiring intensive treatment, is maintained at a sustainable level, even over long periods, while applying minimal durable mobility restrictions.

It is worth noting that while it can be expected that some individuals will naturally reduce their interactions out of fear of illness, our model does not explicitly incorporate this behavior as explored in [33] and [34]. Additionally, we do not consider the concept of "cost of anarchy" as explored in [35].

Finally, we compare simple vaccination policies based on different assigned priorities and intervals between the first and second dose administration. It appears that in the literature, no works explicitly address the combined aspects of rate/ICU occupation control in feedback and vaccination prioritization, exploring them separately. The absence of research specifically addressing the integration of non-pharmaceutical control in feedback and vaccination prioritization highlights a significant gap in the literature, particularly noteworthy given the cur-

rent context of the COVID-19 pandemic, where vaccination campaigns have been implemented alongside other control measures. Our paper aims to fill, at least in part, this gap.

E. Outline of the paper

Section II presents an in-depth examination of the proposed extended SIR model in the absence of public intervention. Section III discusses two control measures to limit the spread of the epidemic: non-pharmaceutical, e.g., lockdown measures, and pharmaceutical interventions, i.e., vaccination prioritization. The impact of controlling the infection rate or exerting control on hospitalizations and ICU occupancy through mobility reduction measures are explored in Sections IV and Section V, respectively. In Section VI, we support our modeling choices by comparing the performance of our *simple* control strategies with optimal control. We perform extensive simulations and a thorough discussion for a *reference* scenario inspired by the COVID-19 pandemic in Section VII. Section VIII concludes the article. We provide a Supplemental Material [5] where there is a more comprehensive exposition of the model, and we include details on the data-driven derivation of the $f_{r,p}$ distributions and the choice of parameters of the reference scenario.

II. BASE MODEL

We start by describing a base version of our compartmental model to describe the spread of a disease in a non-homogeneous population of size N in the absence of any intervention (either pharmaceutical or non-pharmaceutical).

Socio-demographic groups are described by the joint distribution $f_{r,p}$ related to the risk exposure r (which corresponds to the individuals' contact rate) and the death probability p of the individuals.

We consider six epidemiological states: let $S_{r,p}(t)$, $I_{r,p}(t)$, $M_{r,p}(t)$, $H_{r,p}(t)$, $T_{r,p}(t)$, and $D_{r,p}(t)$ denote the number of individuals characterized by (r, p) who at time t are susceptible, infected, immune, hospitalized, under intensive treatment and dead, respectively.

The system presented here can be derived from stochastic processes, as in [36]. Thus there exists an underlying individual-based model in which all the states have a probabilistic and statistical interpretation. In particular, the amount of time spent by an individual in the infected, hospitalized, intensive therapy, the immune compartment is exponentially distributed with mean values $1/\gamma$, $1/\phi$, $1/\tau$, $1/\mu$, respectively. We utilize a set of ordinary differential equations to describe the system dynamics. Figure 1 visually depicts the transitions between different compartments and illustrates the flow of individuals within the system. The transitions between different states in the epidemiological model can be described as follows:

- Susceptible to Infected: Susceptible individuals (S) become Infected (I) when they come in contact with infected individuals. The corresponding transition rate depends on the contact rate (risk exposure r) and the number of infected individuals in the population.

- Infected to Immune: Infected individuals (I) can recover from the disease and acquire immunity, transitioning to the iMmune state (M). The *recovery* rate governs the transition and depends on the average infection duration before recovery.

- Infected to Hospitalized: Some Infected individuals (I) may develop severe symptoms and require Hospitalization (H). Various factors influence the corresponding transition rate, such as the healthcare capacity, the proportion of infected individuals needing hospital care, and also disease severity linked to the *fragility* of individuals.

- Hospitalized to Under Intensive Treatment: Hospitalized individuals (H) who require intensive care Treatment may be transferred to the intensive therapy state (T). The corresponding rate depends on factors such as the availability of intensive care units and the duration of hospitalization before the transfer to ICU.

- Under Intensive Treatment to Deceased: Unfortunately, some infected individuals under intensive Treatment (T) may succumb to the disease and move to the Deceased state (D).

It is important to note that the specific transition rates between states are governed by the model's parameters, which can be estimated based on empirical data or derived from previous studies. These transition dynamics capture the progression of the disease within the population and are crucial for understanding the spread and impact of the epidemic. In the supplemental material (sec. I-C-1), we show how direct transitions $I \to D$ and $H \to D$ can be added to the model.

More precisely, the following set of ordinary differential equations describes the system dynamics:

$$\dot{S}_{r,p}(t) = -\sigma(t)\left(\sum_{r',p'} r' I_{r',p'}(t)\right)\frac{r S_{r,p}(t)}{\sum_{r',p'} r' N f_{r',p'}} + \mu M(t)$$

$$\dot{I}_{r,p}(t) = \sigma(t)\left(\sum_{r',p'} r' I_{r',p'}(t)\right)\frac{r S_{r,p}(t)}{\sum_{r',p'} r' N f_{r',p'}} - \gamma I_{r,p}(t)$$

$$\dot{H}_{r,p}(t) = \gamma p_{r,p}^{IH} I_{r,p}(t) - \phi H_{r,p}(t)$$

$$\dot{T}_{r,p}(t) = \phi p_{r,p}^{HT} H_{r,p}(t) - \tau T_{r,p}(t)$$

$$\dot{D}_{r,p}(t) = \tau p_{r,p}^{TD}(t) T_{r,p}(t)$$

$$\dot{M}_{r,p}(t) = \gamma(1 - p_{r,p}^{IH})I_{r,p}(t) + \phi(1 - p_{r,p}^{HT})H_{r,p}(t)$$
$$+ \tau(1 - p_{r,p}^{TD}(t))T_{r,p}(t) - \mu M(t) \quad\quad (1)$$

where $\sigma(t) \geq 0$ represents all exogenous (uncontrolled) factors changing the infection strength (e.g., seasonal effects). In this paper, we will assume for simplicity that $\sigma(t) = \sigma$ is constant.

The total (uncontrolled) rate of new infections is equal to:

$$\lambda_U(t) = \sigma(t)\left(\sum_{r,p} r I_{r,p}(t)\right)\frac{\sum_{r,p} r S_{r,p}(t)}{\sum_{r,p} r N f_{r,p}}.$$

The total number of susceptible people is $S(t) = \sum_{r,p} S_{r,p}(t)$. Similarly, we introduce the total number of people in the other compartments: $I(t)$, $H(t)$, $T(t)$, $M(t)$, $D(t)$. Probabilities $p_{r,p}^{IH}$, $p_{r,p}^{HT}$ and $p_{r,p}^{TD}(t)$ denote the probability that an individual
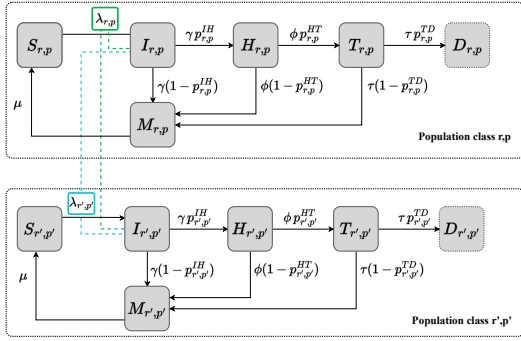
Figure 1. Schematic representation of the proposed model.

of type (r, p) moves between the two compartments indicated in the superscript. We make probability $p_{r,p}^{TD}(t)$ depend on $T(t)$, i.e., on the instantaneous total number of people in ICUs since the death probability dramatically increases when ICUs are saturated. Denoted with $\widehat{T}$ the number of available ICUs, when $T(t) \leq \widehat{T}$, the overall death probability of an infected person is assumed to be equal to p:

$$p_{r,p}^{IH} \cdot p_{r,p}^{HT} \cdot \hat{p}_{r,p}^{TD} = p \qquad \text{if } T(t) \leq \widehat{T}, \qquad (2)$$

where $\hat{p}_{r,p}^{TD}$ is the probability to transit from state T to state D in 'normal' conditions, i.e., when $T(t) \leq \widehat{T}$. Therefore, $p_{r,p}^{TD}(t) = \hat{p}_{r,p}^{TD}$ as long as $T(t) \leq \widehat{T}$.

When $T(t) > \widehat{T}$, we assume that the death probability of people who cannot receive treatment is increased by a factor θ, hence $p_{r,p}^{TD}(t)$ is dynamically adjusted as follows:

$$p_{r,p}^{TD}(t) = \hat{p}_{r,p}^{TD}\frac{\widehat{T}}{T(t)} + \min\{1, \theta \cdot \hat{p}_{r,p}^{TD}\}\frac{T(t) - \widehat{T}}{T(t)}. \quad (3)$$

We consider the case in which individuals might lose immunity with rate μ, thus becoming susceptible again. It should be noticed that the mass preservation $\dot{S}_{r,p}(t) + \dot{I}_{r,p}(t) + \dot{M}_{r,p}(t) + \dot{H}_{r,p}(t) + \dot{T}_{r,p}(t) + \dot{D}_{r,p}(t) = 0$ holds for all $t \geq 0$.

References as [36]–[40] explore SIR-like models with various extensions, including population heterogeneity, additional compartments, and considerations of specific epidemics like COVID-19. They provide insights into such extended SIR models' dynamics and control measures. Unlike [41], our model does not distinguish between infected individuals who remain undetected and those who are detected, nor does it consider this distinction for those who recover. Nonetheless, our proposed model introduces several innovative features that are summarized in the following three remarks.

Remark 1 (Heterogeneity of population in terms of fatality rate and risk exposure). *At the country level, there are substantial differences in population characteristics, including age distribution, general state of health, and frequency of interpersonal interactions. These differences in population contact patterns can potentially influence disease transmission and accelerate the outbreak. Unique distributions, denoted as $f_{r,p}$, for different countries were derived from data on contact patterns and case fatality rates. For more information on*

how these distributions were determined and to see several examples (e.g. Italy, China), see Supplemental Material [5].

The continuous model used in this study can be interpreted as a mean field approximation of an epidemic model that operates over a dynamic network [43]–[45]. According to this interpretation, the risk exposure parameter represents the average number of contacts (per time unit) an individual experiences with others over a fixed time window. Therefore it can be seen as the degree of the corresponding node within a network, in which nodes represent individuals, and the edges represent the contacts between them. Note that pairs of individuals establishing contacts are randomly selected, as for the configuration model. This approach allows us to understand the dynamics of epidemics in terms of the interactions between individuals in a network setting.

Remark 2 (Quadratic dependence on the risk exposure r). *Note that individuals with large r, i.e., pronounced social attitudes, represent at the same time the component of the population with the highest risk of infection and the highest chance of transmitting the disease. Therefore, the "impact" of every individual to the spread of the infection depends quadratically on r.*

Remark 3 (Edge-perspective analysis). *Defining $\widetilde{I}(t) = \sum_{r,p} r I_{r,p}(t)$ as the number of infected contacts, multiplying the first and second equation in (1) by r and summing over r and p, we obtain $\dot{\widetilde{I}}(t) = \gamma(\mathcal{R}(t) - 1)\widetilde{I}(t)$ where $\mathcal{R}(t) = \frac{\sigma \sum_{r,p} r^2 S_{r,p}(t)}{\gamma \sum_{r,p} r N f_{r,p}}$.*

At early stages of epidemic, we can approximate $S_{r,p}(t) \approx N f_{r,p}$ (see Remark 4), obtaining: $\dot{\widetilde{I}}(t) = \gamma(\mathcal{R}_0 - 1)\widetilde{I}(t)$ where we define the related basic reproduction number $\mathcal{R}_0 = \frac{\sigma}{\gamma}\mathbb{E}[r^2]/\mathbb{E}[r]$. As it is clear from the system of equation describing the evolution of the state variables, an edge-perspective analysis provides a fundamental tool to study the dynamics as a natural generalization of the SIR model.

The system of equations (1) can be greatly simplified when $S_{r,p}(t) \approx N f_{r,p}$, and this is instrumental for our subsequent analysis. Indeed:

Remark 4. *Observe that whenever we can find a time interval $[0, T]$ in which we have $\frac{S_{r,p}(t)}{N f_{r,p}} \approx 1 \; \forall r, p, t \in [0, T]$, then Eq. (1) can be dramatically simplified (i.e., linearized) by replacing $S_{r,p}(t)$ with $N f_{r,p}$ on the r.h.s. In particular, in such a case we can set: $\lambda_U(t) \approx \overline{\lambda}_U(t) := \sigma(t)\left(\sum_{r,p} r I_{r,p}(t)\right)$. Now, since by construction we have $S_{r,p}(t) \leq N f_{r,p} \; \forall t, r, p \lambda_U(t) \leq \overline{\lambda}_U(t) \; \forall t$ and $S_{r,p}(0) = N f_{r,p} \; \forall r, p$, denoted with $\mathbb{E}[r] = \sum_{r,p} r f_{r,p}$ the average risk exposure, from Eq. (1) we get*

$$S_{r,p}(t) = N f_{r,p} - \int_0^t \lambda_U(\tau)\frac{r S_{r,p}(\tau)}{N\mathbb{E}[r]}\mathrm{d}\tau + \int_0^t \mu M(\tau)d\tau$$

$$\geq N f_{r,p}\left[1 - \int_0^t \overline{\lambda}_U(\tau)\frac{r}{N\mathbb{E}[r]}\,d\tau\right] + \int_0^t \mu M(\tau)d\tau$$

Therefore, as long as it holds:

$$\max_r \int_0^t \overline{\lambda_U}(\tau)\frac{r}{N\mathbb{E}[r]}\mathrm{d}\tau \ll 1$$

4

we can approximate $S_{r,p}$ with $Nf_{r,p}$ for every (r,p). Lastly, observe that $\int_0^t \overline{\lambda_U}(\tau) \frac{r}{N\mathbb{E}[r]} d\tau$ is an upper bound to the fraction of individuals in class (r,p) who got infected in $[0,t)$.

To check numerically the limits of the validity of approximation $\frac{S_{r,p}(t)}{Nf_{r,p}} \approx 1$, we consider our reference scenario (see Table IV in [5]) related to the Italian population with $N = 60$ million, letting the epidemic evolve uncontrolled. In Fig. 2 we compare the exact solution of Eq. (1) (thick line) with the approximate solution in which $S_{r,p}(t)$ remains fixed and equal to $Nf_{r,p}$ (thin lines). As expected, $I(t)$, $M(t)$, $D(t)$ grow exponentially in the approximate solution (note the log vertical scale), matching the exact solution over an initial time window in which the total number of infected, roughly equal to the total number of individuals $M(t)$ who have recovered, is comparatively small with respect to the total population N (say smaller than 5%). Indeed, when $M(t)$ becomes large, the number $S(t)$ of susceptible starts to drop (roughly after 100 days, with $\mathcal{R}_0 = 2$, or after 200 days, with $\mathcal{R}_0 = 1.5$), and the two solutions deviate from each other. Indeed, in the exact system the epidemic eventually dies out due to herd immunity. Allowing uncontrolled spread of the virus is not sustainable and, in the case of COVID-19, has not been considered a viable option by any developed country. Therefore, this regime is not of interest, the rate of new infections should be controlled and this makes our assumption reasonable.

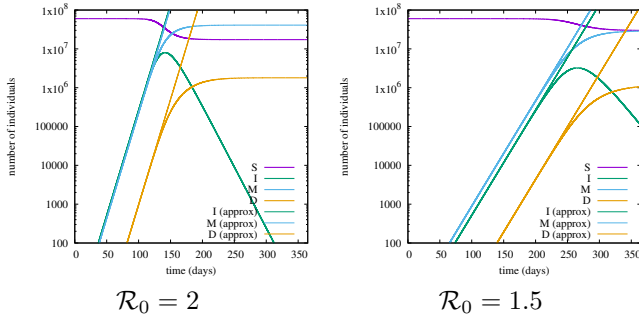$\mathcal{R}_0 = 2$ $\mathcal{R}_0 = 1.5$

Figure 2. Evolution of $S(t)$, $I(t)$, $M(t)$, $D(t)$ in an uncontrolled scenario with $\mathcal{R}_0 = 2$ (left plot), or $\mathcal{R}_0 = 1.5$ (right plot). Comparison between exact solution (thick lines) according to Eq. (1), and approximate solution with $S_{r,p}(t) = Nf_{r,p}$ (thin lines).

III. EPIDEMIC CONTROL

To mitigate the epidemic, several interventions are possible: (a) investments in the public health system, e.g., increasing the available number of ICUs $\widehat{T}$ and hospitalization facilities $\widehat{H}$, (b) non-pharmaceutical interventions, i.e., public health measures preventing and/or controlling virus transmission (sec. III-A); (c) vaccination that aims to reduce both the transmission and clinical severity of the disease (sec. III-B).

Our analysis will focus on quantifying the cost and the impact of different control strategies that jointly exploit non-pharmaceutical interventions and vaccination. In this section, first we formalize the control problems in their most general formulation and then we introduce our *simple* strategies. Indeed, our goal is not to develop a mathematical theory of optimal control for epidemics but to provide a practical framework that informs public policy in controlling the spread

of epidemics. We intend to offer decision-makers a means to compare and evaluate a set of feasible controls, allowing them to make informed choices based on the outcomes and trade-offs associated with different control strategies.

A. Control via non-pharmaceutical interventions

Non-pharmaceutical interventions are measures aimed at controlling the virus by managing certain behaviors in the population, such as using PPE (e.g. masks), implementing lockdowns, promoting telework, to name a few. In our framework, we do not model the effects of social distancing and other countermeasures at a microscopic (class-specific) level. Instead, we summarize their effects by a single control parameter $\rho(t)$ that scales down the overall rate of potential (uncontrolled) new infections.

Specifically, we include the control in the model described by Eq. (1) by setting the actual intensity of new infections $\lambda(t)$ equal to $\frac{\lambda_U(t)}{\rho(t)}$, leading to an effective reproduction number:

$$\mathcal{R}^\rho(t) = \frac{\sigma}{\rho(t)\gamma} \frac{\sum_{r,p} r^2 S_{r,p}(t)}{\sum_{r,p} Nrf_{r,p}}.$$

In this scenario, we will distinguish two main contributions to the cost: the social and the economic cost. It is crucial to note that the distinction between social and economic costs is not always clear-cut. Lockdown measures, while aimed at minimizing the social cost of the pandemic in terms of reducing deaths, have economic repercussions. Similarly, the economic cost of the pandemic, such as job losses and reduced economic activity, has social implications. Moreover, for technical reasons in some cases we add a third component related to healthcare stress to the cost. Accordingly we define:

(a) the <u>social cost</u>, evaluated in terms of the cumulative number of deaths as defined [46];

(b) the <u>stress on the healthcare system</u> induced by the disease's severity;

(c) the <u>economic cost</u> $\mathfrak{C} = \mathfrak{C}(\rho)$, since widespread lockdowns cause a massive negative impact on the economy.

In Figure 3 we show some examples of economic costs as a function of the control parameter ρ. The economic costs are assumed monotone increasing with $\mathfrak{C}(1) = 0$. In the optimal
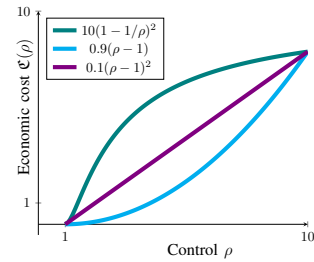

Figure 3. Examples of economic costs as a function of control parameter

control formulation (see [2] and reference therein) a terminal cost is generally defined by taking a linear combination of the above costs and the policymaker aims at solving the following

optimization problem:

$$\rho^\star(t_{\max}) = \underset{\rho:[0,t_{\max}]\to[1,\infty)}{\text{argmin}} \kappa_1 \frac{D(t_{\max})}{N} +$$

$$+ \int_0^{t_{\max}} \left[\kappa_2 \left(\frac{T(t)}{N} \right)^\zeta + \kappa_3 \mathfrak{C}(\rho(t)) \right] \mathrm{d}t$$

$$\text{s.t. dynamics in Eq. (1)} \tag{4}$$

where the exponent ζ is typically assumed greater than 1, while $\kappa_1, \kappa_2, \kappa_3 \geq 0$ are the parameters that weigh the social, the healthcare stress and the economic costs in the objective function, according to how much one values one over the others.

Similarly to [32], we consider two *simple* control strategies:

Rate Control (Control on New Infections)**.** The rate of new infections is tightly controlled and kept at a certain desired level λ_C. The main goal is to avoid congestion in the sanitary system by controlling the circulation of the virus.

HT Control (Control on Hospitalizations and intensive Therapy occupancy)**.** It directly uses the current level of hospitalization/intensive-therapy occupancy as a control signal. Such a signal is readily available and less noisy than the rate of new infections. However, it may introduce a delay in the control loop, which may endanger system stability.

B. Control via vaccination prioritization

1) Modeling the effect of vaccinations: In addition to non-pharmaceutical interventions, vaccination campaigns are a critical measure to contain the virus. Here, we incorporate the effect of vaccinations in our proposed model.

Vaccines are assumed to guarantee partial protection. According to classification in [47], we consider two efficacy descriptors: reduction in the probability of becoming infected (vaccine efficacy on susceptibility) and reduction in the pathogenicity (vaccine efficacy to prevent or diminish symptoms). For simplicity, we neglect the vaccine response transient, and we consider a single type of vaccine administered in two doses separated by a fixed interval of Δ days. We assume that the administration rate of either dose is fixed, equal to ξ, so the entire population can be potentially vaccinated (with two doses) after $\mathcal{T}_v$ days. Hence we set $\xi = N/(\mathcal{T}_v - \Delta)$. Let $\mathsf{VE}^1, \mathsf{VE}^2$ be the vaccine efficacy on susceptibility after one or two doses, respectively. Moreover, we assume that mortality is reduced by a factor q_{post} after a single dose of vaccine.

We assume that N^{novax} people refuse vaccination uniformly distributed over the population. Their state evolution is still described by equations (1). Let $S_{r,p}^{\text{novax}}(t)$ be the number of no-vax people in class (r,p) who are still susceptible at time t.

We describe the dynamics assuming individuals do not return to the susceptible state after infection or vaccination. This extension is not difficult, but we omit it for brevity.

Vaccinations require the addition of a few more compartments: Let $V_{r,p}^{1m}(t)$ be the number of people in class (r,p) who have received just the first dose, which is already effective against the virus, i.e., they can no longer be infected. Let $V_{r,p}^{1s}(t)$ be the number of people in class (r,p) still susceptible after receiving just the first dose. Let $V_{r,p}^{2m}(t)$ be the number of people in class (r,p) who have received both doses and are immune. At last, let $V_{r,p}^{2s}(t)$ be the number of people in class (r,p) who have received both doses but are still susceptible. Due to strict prioritization among classes, a given class (r,p) receives the first dose at full rate ξ only within a specific time window: $[\mathcal{T}_{r,p}^{\min}, \mathcal{T}_{r,p}^{\max}]$ (to be specified later):

$$\xi_{r,p}^{(1)}(t) = \begin{cases} 0 & t < \mathcal{T}_{r,p}^{\min} \\ \xi & \mathcal{T}_{r,p}^{\min} \leq t < \mathcal{T}_{r,p}^{\max} \\ 0 & t \geq \mathcal{T}_{r,p}^{\max} \end{cases}$$

Let $V_{r,p}^1(t) = \int_{t-\Delta}^t \xi_{r,p}^{(1)}(t)\mathrm{d}t$ be the number of people in class (r,p) who have received just the first dose of vaccine at time t. The second dose of vaccine is administered at a rate

$$\xi_{r,p}^{(2)}(t) = \frac{V_{r,p}^{1s}(t) + V_{r,p}^{1m}(t)}{V_{r,p}^1(t)} \xi_{r,p}^{(1)}(t - \Delta)$$

only to individuals who have received the first dose and have not been infected in the meanwhile. At last, let

$$\widehat{S}(t) = \sum_{r,p} r(S_{r,p}(t) + V_{r,p}^{1s}(t) + V_{r,p}^{2s}(t) + S_{r,p}^{\text{novax}}(t))$$

be the total number of susceptible edges at time t. Note that $\lambda(t) = \frac{\sigma}{\rho(t)} \left(\sum_{r,p} r I_{r,p}(t) \right) \frac{\widehat{S}(t)}{\mathbb{E}[r]N}$. Since people who receive at least one dose are less likely to die, we need to keep track of them, hence vaccinated people who get infected traverse a separate chain of compartments $I_{r,p}^v(t), H_{r,p}^v(t), T_{r,p}^v(t)$ with respect to those who do not receive any dose (see Figure 11 in the Supplemental Material [5]). Dynamics governing the evolution of $H_{r,p}^v(t), T_{r,p}^v(t)$ are analogous to those in (1) with the only difference that $p_{r,p}^{TD}(t)$ is replaced by $p_{r,p}^{TD}(t)/q_{\text{post}}$. The complete system of differential equations is an extension of (1), it is omitted here for brevity and reported in sec. V of [5] The vaccination window for each class is computed based on the class priority: $\mathcal{T}_{r,p}^{(1),\max} = \inf\{t : S_{r,p}(t) = 0\}$; $\mathcal{T}_{r,p}^{(1),\min} = \max_{(r',p') \in HP(r,p)}\{\mathcal{T}_{r',p'}^{\max}\}$, where $HP(r,p)$ is the set of classes with higher priority than (r,p).

As final consideration, we emphasize that the rate ξ is typically limited by the capacity of both the vaccine production and distribution infrastructure. However, to increase the effectiveness of the vaccination campaign, the vaccination rate must always be as high as possible under the above conditions.

2) Vaccine prioritization: The vaccination policy involves assigning a priority to each (r,p) class therefore determining which classes should be given priority.

Remark 5. *Any possible prioritization (permutation) $\pi_{(r,p)}$ of classes (r,p) corresponds to a different vaccination policy, The optimal control problem defined in Eq. (4) can be easily extended to take into considerations vaccinations as follows:*

$$(\rho^\star(t_{\max}), \pi_{(r,p)}^*) = \underset{\substack{\rho:[0,t_{\max}]\to[1,\infty) \\ \pi_{(r,p)}}}{\text{argmin}} \kappa_1 \frac{D(t_{\max})}{N} +$$

$$+ \int_0^{t_{\max}} \left[\kappa_2 \left(\frac{T(t)}{N} \right)^\zeta + \kappa_3 \mathfrak{C}(\rho(t)) \right] \mathrm{d}t$$

s.t. dynamics in (9), Supplemental Material. (5)

Again, we consider two *simple* vaccination policies the Most Vulnerable First (MVF) and the Most Social First (MSF):

MVF Policy (Most Vulnerable First). The MVF policy aims to protect the most clinically vulnerable people, with the goal of minimizing the number of deaths. It prioritizes classes with a higher value of p. For the same p, classes with higher r are vaccinated first.

MSF Policy (Most Social First). The MSF policy prioritizes people with a high contact rate, aiming to minimize the force of infection. Classes with a higher value of r are prioritized. For the same r, classes with higher p are vaccinated first.

The MSF policy is similar in spirit to the degree-based vaccination policy in contact networks [48], which targets the high-degree nodes first before moving on to lower-degree nodes. The interval Δ is another design parameter: prolonging the interval between doses, say from 3 to 12 weeks, might be a sensible choice under limited vaccine supplies, de facto minimizing hospitalization and deaths, especially when the efficacy of the first dose is sufficiently high.

IV. CONTROL ON NEW INFECTIONS

In this section, we show that if function $\mathfrak{C}(\cdot)$ is convex, we can devise a simple strategy to minimize the overall economic cost. As already observed, a key role in the epidemic dynamics is played by $\widetilde{I}(t)$, which, roughly speaking, represents the number of potentially infected contacts (see Remark 3). Thus, a sensible strategy is to control such a quantity. In our derivations, we assume that $S_{r,p}(t) \approx N f_{r,p}$, see Remark 4.

This assumption allows for simplifications in the mathematical modeling and analysis. Indeed, given the definition of $\widetilde{I}(t)$, multiplying the second equation in Eq. (1) by r and summing over r and p, we get:

$$\dot{\widetilde{I}}(t) = \gamma \left(\frac{\sigma}{\rho(t)\gamma} \frac{\sum_{r,p} r^2 S_{r,p}(t)}{\sum_{r,p} N f_{r,p}} - 1 \right) \widetilde{I}(t).$$

under the assumption $S_{r,p}(t) \approx N f_{r,p}$, and defining $\mathcal{R}^\rho(t) = \frac{\mathcal{R}_0}{\rho(t)}$, we obtain the equation:

$$\dot{\widetilde{I}}(t) = \gamma \left(\frac{\mathcal{R}_0}{\rho(t)} - 1 \right) \widetilde{I}(t) = \gamma \left(\mathcal{R}^\rho(t) - 1 \right) \widetilde{I}(t). \quad (6)$$

A. Minimizing the economic cost in a fixed window

Fixing a target value $\widetilde{I}^\star$ for $\widetilde{I}(t)$, to be met within a prefixed a time horizon $t_{\max}$, Proposition 1 establishes optimality conditions.

Proposition 1. *Let $\mathfrak{C}(\rho)$ be a monotone increasing and convex function in $\rho \in [1, +\infty]$ and assume $S_{r,p}(t) \approx N f_{r,p}$. Among all trajectories, such that $\widetilde{I}(t_{\max}) = \sum_{r,p} r I_{r,p}(t_{\max}) = \widetilde{I}^\star$, the one that minimizes the overall economic cost in $[0, t_{\max}]$, is the one corresponding to:*

$$\mathcal{R}^\rho(t) = 1 + \frac{1}{\gamma} \log \left(\widetilde{I}^\star / \widetilde{I}(0) \right) \quad \forall t \in [0, t_{\max}],$$

and,

$$\rho(t) = \frac{\sigma}{\gamma} \frac{\mathbb{E}[r^2]}{\mathbb{E}[r]} \left[1 + \frac{1}{\gamma t_{\max}} \log \left(\widetilde{I}^\star / \widetilde{I}(0) \right) \right]^{-1} \quad \forall t \in [0, t_{\max}].$$

Proof: Consider Eq. (6) and note that the unique solution of the associated Cauchy problem with initial condition $\widetilde{I}(0)$ is given by: $\widetilde{I}(t) = \widetilde{I}(0) \exp \left(\gamma \int_0^t (\mathcal{R}^\rho(\tau) - 1) \, d\tau \right)$. Imposing the constraint $\widetilde{I}(t_{\max}) = \widetilde{I}^\star$ leads to:

$$\frac{1}{t_{\max}} \int_0^{t_{\max}} \mathcal{R}^\rho(\tau) d\tau = 1 + \frac{1}{\gamma t_{\max}} \log \left(\widetilde{I}^\star / \widetilde{I}(0) \right). \quad (7)$$

Now, focusing on a generic trajectory satisfying Eq. (7), we have: $\frac{1}{t_{\max}} \int_0^{t_{\max}} \mathfrak{C}(\rho(\tau)) d\tau = \frac{1}{t_{\max}} \int_0^{t_{\max}} \chi(\mathcal{R}^\rho(\tau)) d\tau$ with $\chi = \mathfrak{C} \circ \rho$, and $\rho(\mathcal{R}^\rho) = \frac{\sigma \mathbb{E}[r^2]}{\gamma \mathbb{E}[r] \mathcal{R}^\rho(t)}$. Since $\mathfrak{C}$ is a monotonic increasing and convex function in $\rho \in [1, +\infty]$ then χ is a convex function over its domain, and by Jensen inequality, we conclude $\frac{1}{t_{\max}} \int_0^{t_{\max}} \chi(\mathcal{R}^\rho(\tau)) d\tau \geq \chi \left(\frac{1}{t_{\max}} \int_0^{t_{\max}} \mathcal{R}^\rho(\tau) d\tau \right)$ Therefore, from Eq. (7) the choice given by $\rho(t) = \frac{\sigma \mathbb{E}[r^2]}{\gamma \mathbb{E}[r]} \left[1 + \frac{1}{\gamma t_{\max}} \log \left(\widetilde{I}^\star / \widetilde{I}(0) \right) \right]^{-1}$, $\forall t \in [0, t_{\max}]$ minimizes the cost. ∎

Observe that the economic cost of previously defined optimal policy monotonically decreases while increasing the target $\widetilde{I}^\star$.

Corollary 1. *Under the assumptions that $\mathfrak{C}(\rho)$ is a monotone increasing and convex function and $S_{r,p}(t) \approx N f_{r,p}$, among all control strategies that maintain the number of infected less than or equal the initial value $\widetilde{I}(0)$, the overall economic cost is minimized when $\mathcal{R}^\rho(t)$ is kept equal to 1.*

Proof: From Proposition 1 we have that among all strategies guaranteeing $\widetilde{I}(t_{\max}) = \widetilde{I}(0)$, the one forcing $\mathcal{R}^\rho(t) = 1$ is cost-optimal. The proof is completed by observing that such a strategy guarantees $\widetilde{I}(t) \leq \widetilde{I}(0)$ for every $t \in [0, t_{\max}]$. ∎

Remark 6. *$\mathcal{R}^\rho(t) = 1$ can be achieved by controlling the rate of new infections and maintaining it equal to the target $\lambda_C = \gamma \widetilde{I}(0) \mathbb{E}[r]/\mathbb{E}[r^2]$. The resulting control function is $\rho(t) = \lambda_U(t-\varepsilon)/\lambda_C = \lambda(t-\epsilon)\rho(t-\varepsilon)/\lambda_C$, where ε is an arbitrarily small positive constant.*

In conclusion, given an initial condition $\widetilde{I}(0)$, a maximum allowable number of infected contacts $\widetilde{I}^\star$ and a time horizon $t_{\max}$, if the goal is to keep $\widetilde{I}(t) \leq \widetilde{I}^\star \quad \forall t \in [t^\star, t_{\max})$, with $t^\star$ as small as possible, the following strategy appears to be the natural answer: if $\widetilde{I}^\star > \widetilde{I}(0)$, set $\mathcal{R}^\rho(t) = 1 + \frac{1}{\gamma t_{\max}} \log \left(\widetilde{I}^\star / \widetilde{I}(0) \right), \forall t \in [0, t_{\max}]$. This strategy, indeed, minimizes the economic cost in $[0, t_{\max}]$, among all strategies that guarantee $\widetilde{I}(t) \leq \widetilde{I}^\star, \forall t \in [0, t_{\max}]$, (i.e., $t^\star = 0$). If, instead, $\widetilde{I}^\star < \widetilde{I}(0)$, we can not guarantee $t^\star = 0$, and therefore to minimize $t^\star$ it is necessary to minimize $\mathcal{R}^\rho(t)$ in $[0, t^\star)$ and then to set $\mathcal{R}^\rho(t) = 1, \forall t \in [t^\star, t_{\max}]$. Indeed, this is the strategy that minimizes the economic cost in $[0, t_{\max}]$, among all strategies minimizing $t^\star$. Previous arguments can be formalized in the following proposition.

Proposition 2. *Given $\widetilde{I}(0)$, $\widetilde{I}^\star$ and $t_{\max}$, whenever our goal is to keep $\widetilde{I}(t) \leq \widetilde{I}^\star, \forall t \in [t^\star, t_{\max})$, with $t^\star$ as small as possible, the strategy described above is cost-optimal.*

It is worth remarking that the optimality criteria depend on various factors, including the dynamics of the system,

the objective function, and the constraints. In the context of our study, the choice of time horizon $t_{\max}$ plays a crucial role. If $t_{\max}$ is set too low, it might limit the effectiveness of the control measures. We emphasize that the selection of $t_{\max}$ should be carefully considered based on the specific context and dynamics of the epidemic under investigation. The parameter $\tilde{I}^\star$, instead, represents the maximum admissible number of infected over the considered time horizon $t_{\max}$ and is indissolubly related to the transmission rate λ. It represents the number of infected it is possible to sustain (in a country, for example). This again showcases the tradeoffs between social cost (in terms of deaths) and economic cost (the entity of restriction measures), small values of $\tilde{I}^\star$ would result in a small number of deaths but also in a high economic cost. Our analysis will provide insights for a fixed value of $\tilde{I}^\star$, chosen by the decision maker according to the tradeoff between social and economic cost and the acceptable number of infected by the overall healthcare infrastructure. We acknowledge that this choice could potentially be optimized to minimize the cost, and while we do not explicitly optimize it in our study, we will discuss the implications of different target numbers and their impact on the control measures (see sec. IV-C).

B. Rate Control with feedback delay

Policymakers cannot instantaneously react to changes in the rate of new infections due to several reasons: i) new infections are discovered by tests performed several days after infection, and high-risk individuals are more likely to undergo testing [49], ii) new regulations take time to be introduced and become effective, iii) decisions are based on trends obtained by averaging epidemiological curves, iv) the actual process of new infections in unknown (think of asymptomatic but infectious people). Consequently, the measured process is a delayed, noisy subsample of the actual process. Therefore, we consider the case in which the actual, instantaneous effectiveness of mobility restrictions, modeled by $\rho(t)$, is given by: $\rho(t) = \max\left\{1, \frac{\int \mathfrak{f}_d(\tau)\lambda_U(t-\tau)\,\mathrm{d}\tau}{\lambda_C}\right\}$ where $\mathfrak{f}_d(\cdot)$ is a feedback delay distribution.

One of our main results is that the system becomes unstable if the feedback delay is too large with respect to $1/\gamma$ (the average time in the infectious state). To simplify the analytical derivations, we start with the case of deterministic feedback delay of constant duration d (days). Then we extend the result to a delay distribution $\mathfrak{f}_d$.

Theorem 1 (Stability analysis with constant delay). *Assume*

$$\rho(t) = \max\left\{1, \frac{\lambda_U(t-d)}{\lambda_C}\right\} = \max\left\{1, \frac{\lambda(t-d)\rho(t-d)}{\lambda_C}\right\}$$

and $S_{r,p}(t) \approx Nf_{r,p}$. If the delay $d < \frac{\pi}{2}\gamma$ then the system is locally stable, otherwise the system is unstable.

Proof: Since under the assumption $S_{r,p}(t) \approx Nf_{r,p}$, the equation governing the evolution of the number of infected edges under delayed rate control becomes:

$$\dot{\tilde{I}}(t) = \frac{\tilde{I}(t)}{\tilde{I}(t-d)}\lambda_C \frac{\mathbb{E}[r^2]}{\mathbb{E}[r]} - \gamma\tilde{I}(t) \tag{8}$$

System stability can be analyzed by considering small perturbations around the equilibrium point $\tilde{I}^* = \frac{\lambda_C}{\gamma}\frac{\mathbb{E}[r^2]}{\mathbb{E}[r]}$: $\tilde{I}(t) = \tilde{I}^* + \eta(t)$, with $\eta(t) \ll \tilde{I}^*$. Exploiting the approximation $\frac{1}{1+x} \sim 1 - x$, when $x \approx 0$, from (8) we obtain:

$$\dot{\tilde{I}}(t) = \gamma\tilde{I}^* \frac{1 + \frac{\eta(t)}{\tilde{I}^*}}{1 + \frac{\eta(t-d)}{\tilde{I}^*}} - \gamma(\tilde{I}^* + \eta(t)) \approx -\gamma\eta(t-d)$$

where we have discarded the second-order term $\eta(t)\eta(t-d)$. We end up with the simple differential equation with delay:

$$\dot{\eta}(t) = -\gamma\,\eta(t-d) \tag{9}$$

Taking the Laplace transform $\mathcal{L}\{\eta(t)\}$ we obtain $\mathcal{L}\{\eta(t)\} = \frac{\eta(0)}{s+\gamma e^{-sd}}$. Equation (9) admits solutions of the form $\eta(t) = Ae^{bt}\cos(\omega t + \theta)$ under the conditions:

$$\begin{cases} b = -\gamma e^{-bd}\cos(\omega d) \\ \omega = \gamma e^{-bd}\sin(\omega d) \end{cases} \tag{10}$$

While A and θ can take any value, i.e., can be used to match desired values of $\eta(0)$ and $\eta'(0)$, b and ω are uniquely determined by the feedback delay d. Besides the trivial solution $b = \omega = 0$, there exists a stationary solution $b = 0$, $\omega = \gamma$ for the special case $d = \frac{\pi}{2\gamma}$. If $d < \frac{\pi}{2\gamma}$, from the first constraint we have that $b < 0$, corresponding to dumped oscillations. For $\frac{\pi}{2\gamma} < d < \frac{3\pi}{2\gamma}$, we have instead amplifying oscillations ($b > 0$). Therefore, $d = \frac{\pi}{2\gamma}$ is the critical value for stability. ∎

The analysis can be extended to a delay distribution $\mathfrak{f}_d$.

Theorem 2 (Stability analysis with delay distribution). *Assume that $\rho(t) = \max\left\{1, \int \mathfrak{f}_d(\tau)\lambda_U(t-\tau)\,\mathrm{d}\tau/\lambda_C\right\}$ and $S_{r,p}(t) \approx Nf_{r,p}$. Let $\mathcal{Z} = \{z \in \mathbb{C} : z + \gamma\,\mathfrak{F}_d(z) = 0\}$, where $\mathfrak{F}_d(z)$ is the Laplace transform of the delay distribution. Then, if $\mathrm{Re}(z) < 0 \;\forall z \in \mathcal{Z}$, the system is locally stable.*

Proof: Repeating the same approximations as before for small variations around the equilibrium $\tilde{I}^*$, we obtain the differential equation with delay distribution:

$$\dot{\eta}(t) = -\gamma \int \mathfrak{f}_d(\tau)\eta(t-\tau)\,\mathrm{d}\tau \tag{11}$$

Taking the Laplace transform, we get $H(s) = \eta(0)/(s + \gamma\,\mathfrak{F}_d(s))$. Note that when $\mathfrak{f}_d(\tau) = \delta(\tau - d)$, we obtain the case with constant delay. We evince that we need the set of zeros $\mathcal{Z} = \{z \in \mathbb{C} : z + \gamma\,\mathfrak{F}_d(z) = 0\}$ to lie in the left half-plane to ensure stability. ∎

In the following corollaries, whose proof is given in [5] we explore two interesting cases of feedback delay distributions.

Corollary 2 (Exponential delay distribution). *If $\mathfrak{f}_d(\tau) = u(\tau)\delta e^{-\delta(\tau)}$, then the system is always (locally) stable.*

Corollary 3 (Shifted exponential delay distribution). *Let $\mathfrak{f}_d(\tau) = u(\tau - d)\delta e^{-\delta(\tau-d)}$. For any given $\delta > 0$, there exists a critical delay $d^* = \frac{1}{\gamma}f(\delta)$, such that the system is (locally) stable if $d < d^*$, otherwise the system is unstable. As δ grows from 0 to ∞, d^* grows from $1/\gamma$ to $\pi/(2\gamma)$.*

The shifted exponential distribution can represent a system where: i) an exponentially weighted moving average (with parameter δ) is used to estimate the current trend of the

epidemiological curve, ii) some fixed delay d is introduced before the control becomes effective. Our results suggest that system stability is crucially tied (by a factor between 1 and $\pi/2$ that depends on δ) to the mean sojourn time $1/\gamma$ in the infectious state. If d is too large with respect to $1/\gamma$, the control based on the force of infection is prone to instability.

In a finite population system, as time goes on, we can no longer assume that $S_{r,p}(t) \approx N f_{r,p}$, since the number of initially susceptible individuals is progressively reduced by the number of people who get infected (see (1)). Moreover, $S_{r,p}(t)$ can vary because of vaccinations and the finite duration of immunity. Nevertheless, we can still apply the above results by resorting to a *time-scale separation approach*, i.e., by assuming that $S_{r,p}(t)$, though not equal to $N f_{r,p}$, are almost constant at the time scale over which we analyze stability.

Remark 7. *The assumption of a constant number of susceptible individuals is fairly accurate when dealing with dynamics of a large population over a relatively small window of time. In such a case, the rate of infection spread may have a minimal impact on the overall number of susceptible individuals in relative terms (mathematical considerations as in Remark 4 apply). We emphasize that the rate of newly infected people should be sufficiently small to ensure that the total number of infected/recovered people in the considered window is negligible with respect to the number of susceptible individuals.*

Indeed, recall from Remark 3 that the evolution of the total number of infected edges can be written as:

$$\dot{\widetilde{I}}(t) = \gamma \left(\frac{\mathcal{R}(t)}{\rho(t)} - 1 \right) \widetilde{I}(t) \tag{12}$$

where $\mathcal{R}(t) = \frac{\sigma \sum_{r,p} r^2 S_{r,p}(t)}{\gamma \sum_{r,p} r N f_{r,p}}$ is the basic reproduction in the general case. This equation is formally identical to (6) upon substituting $\mathcal{R}_0$ with $\mathcal{R}(t)$. Since our stability results do not depend on $\mathcal{R}_0$, they apply also to a system in which $\mathcal{R}(t)$ can be considered approximately constant at the time scale at which we analyze the system stability (i.e., time scale of $1/\gamma$).
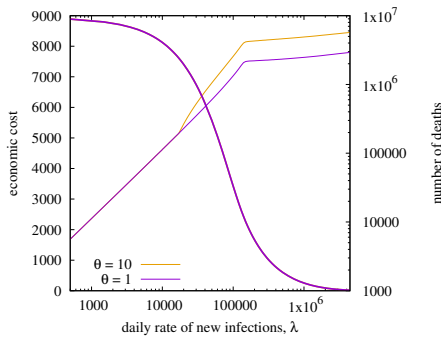
C. Sensitivity Analysis - The impact of λ

Figure 4.   Parametric curves of economic cost vs social cost, as we vary λ, with $\theta \in \{1, 10\}$.

Fig. 4 reports both the economic cost and number of deaths observed over a time horizon $t_{\max} = 1$ year as a function of the control parameter λ. We refer the reader to Table IV

of the Supplemental Material [5] for a detailed description of all the infection-parameters. When controlling the infection rate, the suppression strategy, i.e., minimizing infection rate λ, appears to be the most reasonable choice since it minimizes the number of deaths incurring an almost constant economic cost for, e.g., all values of $\lambda < 10000$. Indeed note that, once the system is stabilized around a fixed infection rate[1] λ^*, the economic cost is the same for any λ^*, as long as $S(t) \approx N$.

In the case of COVID-19, some countries, e.g., China, have adopted the suppression strategy, which is particularly effective when restrictions can be geographically localized to small areas with limited impact on the national economy. Of course, this cannot be a solution in the long term unless the virus is totally eradicated or conditions change, e.g., herd immunity is reached through vaccinations. Indeed, note that all results discussed so far refer to a fixed time horizon $t_{\max} = 1$ year.
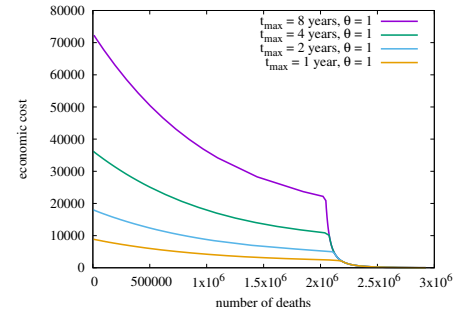

Figure 5.   Parametric curves of economic cost vs social cost, as we vary λ, for different time horizons $t_{\max}$; $\theta = 1$.

To understand how the optimal strategy might change as we increase the time horizon $t_{\max}$, it is convenient to look at the plot in Fig. 5, showing parametric curves of economic cost vs. social cost, as we vary λ, for $t_{\max} = 1, 2, 4, 8$ years. These results have been obtained by running the multi-class model with the parameter θ, representing the increase of mortality due to ICU saturation, equal to 1, putting us in the most favorable conditions (i.e., in the presence of unlimited healthcare facilities) to decide to abandon the suppression strategy. Clearly, under the suppression strategy, the economic cost increases linearly with time, so for $t_{\max}$ large enough, this strategy becomes necessarily suboptimal[2].

Interestingly, curves shown in Fig. 5 can be split into two convex parts connected at the point where the population reaches natural herd immunity (the knee). The consequences of this behavior on the multi-objective function (4), for $\kappa_2 = 0$ and $\kappa_3 = 1$, which is linear with respect to trade-off factor κ_1, are illustrated in Fig. 6 for the case $t_{\max} = 4$ years. We observe that all points between B and C are not Pareto-efficient, hence cannot be optimal solutions for the optimization problem (4). The optimal strategy exhibits a phase transition with respect to κ_1: for small values of κ_1 (social cost

---

[1]Further, note that with proper control, the cost incurred during the transient phase necessary to bring the system to operate at a given λ is negligible with respect to the long-term accumulated cost.

[2]It should be noticed, however, that a finite population model like ours is not adequate to describe a system running for more than, say, a few years.
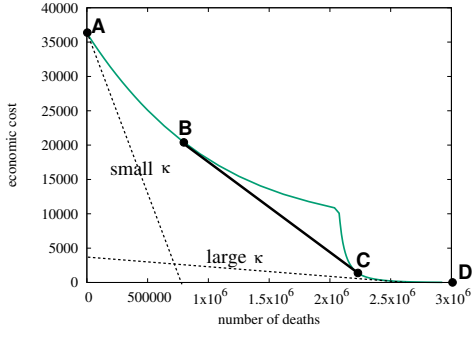
Figure 6. Pareto frontier of the multi-objective function (4) in the case $t_{\max} = 4$ years; $\theta = 1$.

much more important than economic cost), the best strategy is total suppression (point A), whereas for large κ_1 we end up operating beyond the herd immunity knee. Intermediate solutions between A and B also exist, but only for a very small, particular range of κ_1 values.
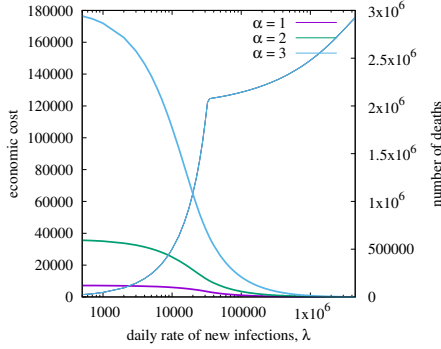

Figure 7. Economic and social costs as a function of controlled rate λ, for fixed $t_{\max} = 4$ years and different values of α.

The particular value of κ_1 at which the phase transition occurs, in addition to the time horizon $t_{\max}$, depends crucially on the exponent α, as one can intuitively understand from Fig. 7, which shows economic and social costs as a function of the controlled rate λ, for fixed $t_{\max} = 4$ years, and different values of the exponent in the economic cost $\alpha = 1, 2, 3$: while the social cost is the same for all α, the economic cost depends dramatically on α. Note that $\alpha = 1$ is the extreme case for the validity of Proposition 1.

Proper values of α to be used in the model are difficult to set. However, the general conclusion remains the same: unless one considers considerably long (but unlikely to be significant) time horizons, the best option always appears to be the minimization of λ. With the parameters of COVID-19, and in particular, for the delta variant, the opposite 'let it rip' strategy in which one tries to achieve the natural herd immunity (while still controlling λ to avoid ICU saturation) produces an unreasonable social cost in terms of deaths. Some countries (like the UK) initially considered this option at the onset of the pandemic but quickly switched back to the suppression strategy after a few months.

Another reason why the 'let it rip' strategy considered so far is perilous is that it relies on the assumption that recovered people are immune forever, i.e., recovery rate $\mu = 0$. In

the case of COVID-19, natural immunity is progressively lost over time, so reinfections are possible about six months after recovery. Even assuming that reinfected people are much less likely to develop a severe form of the disease, we expect a significantly higher social cost when $\mu > 0$. This observation is confirmed by results in Fig. 8, showing economic and social costs for $t_{\max} = 4$ years, mortality reduction after the first exposure $q_{\text{post}} = 10$, and different values of the average sojourn time in the immune state, equal to 6 months (as estimated for COVID-19), 1 year, 2 years, in addition to the optimistic hypothesis $\mu = 0$.
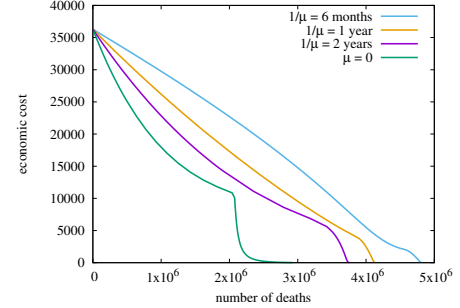

Figure 8. Parametric curves of economic cost vs social cost, as we vary λ, for fixed $t_{\max} = 4$ years and different values of μ. Mortality rate after reinfection is reduced by $q_{\text{post}} = 10$.

Note that at the beginning of the pandemic, the decision of which strategy to adopt was daunting because nobody knew the characteristics of the novel virus and whether effective vaccines could be developed, and after how much time. It was also unknown when and which mutations of the original virus would have replaced the original strain. In later sections, we will bring into the picture these two fundamental factors that have steered the pandemic's evolution after the first year.

V. CONTROL ON HOSPITALIZATIONS AND INTENSIVE THERAPY OCCUPANCY

Recall that, according to the HT strategy, the control variable $\rho(t)$ is directly related to the instantaneous numbers $H(t)$ and $T(t)$ of patients who are currently hospitalized or under intensive treatment, respectively. Many countries have widely adopted this strategy, being particularly simple to implement.

A. Stability analysis

We assume that Hospitals and ICUs have a maximum capacity $\widehat{H}$ and $\widehat{T}$, correspondingly. A maximum level of restrictions $\rho_{\max}$ is applied whenever either $H(t)$ exceeds $H_{\max}$ (with $H_{\max} \leq \widehat{H}$), or $T(t)$ exceeds $T_{\max}$ ($T_{\max} \leq \widehat{T}$). When $H(t) < H_{\max}$ and $T(t) < T_{\max}$, we assume that two control functions $\rho_H : \mathbb{R}^+ \to [1, \infty)$ and $\rho_T : \mathbb{R}^+ \to [1, \infty)$ provide two different levels of restrictions, the larger (i.e. stricter) of which is actually applied: $\rho := \max\{\rho_H \circ H, \rho_T \circ T\}$.

Assumption 1. Let $\rho_H \in C^1[0, H_{\max}]$, $\rho_T \in C^1[0, T_{\max}]$ such that $\rho_H(0) = \rho_T(0) = 1$, $\rho_H(H_{\max}) = \rho_T(T_{\max}) = \rho_{\max}$, with $\inf_{x \in (0, H_{\max})} \dot{\rho}_H(x) > 0$ and $\inf_{x \in (0, T_{\max})} \dot{\rho}_T(x) > 0$.

10

To analyze the system stability under the above type of control, we first assume $S_{r,p}(t) \approx N f_{r,p}$. We will later extend the analysis to the general case through a time-scale separation approach. Under the assumption $S_{r,p}(t) \approx N f_{r,p}$ we have that the total number of infected 'edges' is governed by Eq. (6).

Proposition 3 (Stationary solutions). *Under the assumption $S_{r,p}(t) \approx N f_{r,p}$ and Assumption 1 the stationary solutions satisfy:*

$$H^* = \frac{\gamma}{\phi} \widetilde{I}^* \frac{\mathbb{E}[r \, p_{r,p}^{IH}]}{\mathbb{E}[r^2]}, \quad T^* = \frac{\gamma}{\tau} \widetilde{I}^* \frac{\mathbb{E}[r \, p_{r,p}^{IH} \, p_{r,p}^{HT}]}{\mathbb{E}[r^2]}. \quad (13)$$

Proof: From the definition we have $I_{r,p}(t) = \widetilde{I}(t) \frac{r f_{r,p}}{\mathbb{E}[r^2]}$, $I(t) = \widetilde{I}(t) \frac{\mathbb{E}[r]}{\mathbb{E}[r^2]}$. It should be noted that at equilibrium necessarily $\rho^*(t) = \mathcal{R}_0$ for all t and, by monotonicity of ρ_H and ρ_T, we have one of the following cases:

- $H^* = \rho_H^{-1}(\mathcal{R}_0)$, and $T^* \leq \rho_T^{-1}(\mathcal{R}_0)$;
- $T^* = \rho_T^{-1}(\mathcal{R}_0)$, $H^* \leq \rho_H^{-1}(\mathcal{R}_0)$.

Hence,

$$\widetilde{I}^* = \min\left(\rho_H^{-1}(\mathcal{R}_0) \frac{\phi}{\gamma} \frac{\mathbb{E}[r^2]}{\mathbb{E}[r \, p_{r,p}^{IH}]}, \rho_T^{-1}(\mathcal{R}_0) \frac{\tau}{\gamma} \frac{\mathbb{E}[r^2]}{\mathbb{E}[r \, p_{r,p}^{IH} \, p_{r,p}^{HT}]} \right).$$

Now, from (1), we obtain detailed equilibrium points:

$$I_{r,p}^* = \widetilde{I}^* \frac{r f_{r,p}}{\mathbb{E}[r^2]}, H_{r,p}^* = \frac{\gamma}{\phi} I_{r,p}^* p_{r,p}^{IH}, T_{r,p}^* = \frac{\phi}{\tau} H_{r,p}^* p_{r,p}^{HT}$$

Therefore, summing over (r, p), we get corresponding equilibria for the total number of people hospitalized or under intensive therapy as given by Eq. (13). ∎

Theorem 3 (Stability analysis). *Let ρ_H and ρ_T satisfy Assumption 1 and H^* and T^* be stationary solutions as given in Proposition 3. If at least one of the following conditions is satisfied:*

- $\rho_H(H^*) > \rho_T(T^*)$
- $\rho_T(T^*) \geq \rho_H(H^*)$ and $\phi + \tau \geq \frac{T^* \dot{\rho}_T(T^*) \gamma}{\mathcal{R}_0}$

then the system is locally stable.

Proof: Let us consider small perturbations around the equilibrium point $\widetilde{I}^*$: $\widetilde{I}(t) = \widetilde{I}^* + \widetilde{\eta}(t)$ with $\widetilde{\eta}(t) \ll \widetilde{I}^*$.

We will assume that $0 < H^* < H_{\max}$, and $0 < T^* < T_{\max}$. From Assumption 1, by denoting with $\alpha_H^* = \dot{\rho}(H^*)$ and $\alpha_T^* = \dot{\rho}(T^*)$ we have the following cases.

1) If $\rho_H(H^*) > \rho_T(T^*)$ by continuity we get that $\rho(t) = \rho_H(H(t)) > \rho_T(T(t))$ and assuming initial conditions $H(0) = H^*$, $T(0) = T^*$, after some algebra we get the Laplace transform of $\eta(t)$:

$$\mathcal{L}\{\eta(t)\} = \frac{\eta(0)(s + \phi)}{s(s + \phi) + \frac{H^* \alpha_H^* \phi \gamma}{\mathcal{R}_0}} \quad (14)$$

In this case, the system is always stable for any value of parameters $\phi, \gamma, \mathcal{R}_0$, since the real part of the poles of (14) is always negative. As we increase the amplitude of coefficient $\frac{H^* \alpha_H^* \phi \gamma}{\mathcal{R}_0}$, the real part of the dominating pole moves from 0 to $-\phi$.

2) If $\rho_T(T^*) > \rho_H(H^*)$ then, by continuity, we have $\rho(t) = \rho_T(T(t)) > \rho_H(H(t))$ and, by first order analysis and computing the Laplace transform, we get

$$\mathcal{L}\{\eta(t)\} = \frac{\eta(0)(s + \phi)(s + \tau)}{s(s + \phi)(s + \tau) + \frac{T^* \alpha_T^* \tau \phi \gamma}{\mathcal{R}_0}}$$

The system may be unstable since we obtain in the denominator a third-order equation whose complex solutions can fall in the positive half-plane. In particular, the system is stable when:

$$\phi + \tau \geq \frac{T^* \alpha_T^* \gamma}{\mathcal{R}_0} \quad (15)$$

while it becomes unstable otherwise. Indeed, pure imaginary solutions $s = i\omega$ are roots of the above third order equation when $\omega = \sqrt{\tau \phi}$, while relation (15) is satisfied with equality. ∎

Theorem 3 provides conditions guaranteeing the local stability of the system.

In particular, it is worth remarking that once $H_{\max} \leq \widehat{H}$ has been fixed, condition $\rho_H(H^*) > \rho_T(T^*)$ can always be achieved by arranging a sufficiently large number of available intensive therapy facilities. Indeed, even when $\mathcal{R}_0$ is not perfectly known, it is sufficient to guarantee:

$$\rho_H^{-1}(y) \frac{\phi}{\gamma} \frac{\mathbb{E}[r^2]}{\mathbb{E}[r \, p_{r,p}^{IH}]} < \rho_T^{-1}(y) \frac{\tau}{\gamma} \frac{\mathbb{E}[r^2]}{\mathbb{E}[r \, p_{r,p}^{IH} \, p_{r,p}^{HT}]}$$

for every $\rho_{\min} < y < \rho_{\max}$, i.e. $\frac{\rho_T^{-1}(y)}{\rho_H^{-1}(y)} > \frac{\phi}{\tau} \frac{\mathbb{E}[r \, p_{r,p}^{IH} \, p_{r,p}^{HT}]}{\mathbb{E}[r \, p_{r,p}^{IH}]}$. Observe that the above constraint can be met if

$$T_{\max} > \frac{\phi}{\tau} \frac{\mathbb{E}[r \, p_{r,p}^{IH} \, p_{r,p}^{HT}]}{\mathbb{E}[r \, p_{r,p}^{IH}]} H_{\max} \quad (16)$$

by adopting controllers that satisfy the relationship: $\rho_H(x H_{\max}) \geq \rho_T(x T_{\max}) \quad \forall \, 0 \leq x \leq 1$.

When the number of intensive therapies is, instead, underdimensioned, we have $\rho_H(H^*) > \rho_T(T^*)$, and the system stability essentially depends on the average time spent in hospitals and ICU, through the sum $\phi + \tau$ of transitions rates out of compartments H, T (both are equally important).

Assuming that $S_{r,p}(t)$ are almost constant on the time scale over which stability is studied, the analysis can be extended by replacing the basic reproduction number $\mathcal{R}_0$ with the effective reproduction number $\mathcal{R}(t)$. Indeed, by doing so, the evolution of the total number of infected edges (12) becomes formally identical to (6).

B. Sensitivity Analysis - The impact of $H_{\max}$ and $T_{\max}$

In the same settings as in sec. IV-C, we start analyzing the impact of the maximum tollerable levels of hospitalized and ICU patients $H_{\max}$ and $T_{\max}$ on the system dynamics. Both the implemented controllers are linear.

In all the cases we have set the capacities as $\widehat{H} = 50000$ and $T_{\max} = \widehat{T}$. The choice $T_{\max} = \widehat{T}$ is justified by our previous analysis, according to which the maximization of ratio $T_{\max}/H_{\max}$ favors system local stability around the equilibrium point. Note that our choice of parameters guarantees

local stability also in cases in which the tightest control at the equilibrium point is exerted by intensive therapies occupancy Finally note that, since in our scenario $\frac{\phi}{\tau}\frac{\mathbb{E}[r\,p_{r,p}^{IH}\,p_{r,p}^{HT}]}{\mathbb{E}[r\,p_{r,p}^{IH}]} = 0.331$, we should enforce $T_{\max}/H_{\max} > 0.331$ to guarantee that at the equilibrium point, the tighter control is exerted by hospitalizations.

Figure 9 reports some result. First, we have fixed $T_{\max} = 10000$ and we let $H_{\max}$ vary. In particular we have chosen: $H_{\max} = 20000$ (top left plot), $H_{\max} = 30000$ (top right plot), $H_{\max} = 50000$ (bottom left plot).

Only the first choice for $H_{\max}$ satisfies condition Eq. (16). Note that by reducing $H_{\max}$, we significantly reduce oscillations since the control on hospitalization becomes reactive. Periods in which the tightest control is exerted by hospitalizations/intensive therapy occupancy are highlighted in the figures. In no cases saturation of intensive treatment facilities is observed. Table I complements the previous figure by reporting economic costs (with economic cost exponent $\alpha = 1, 2, 3$) and deaths for all scenarios. In general, more conservative choices of $H_{\max}$ lead to significant reductions in the number of deaths, and in some cases also in the economic cost, as an effect of the reduction of oscillations.

We have also tested, reporting results in Table I), situations in which $T_{\max}/H_{\max}$ is kept fixed equal to two (so to guarantee the satisfaction of condition Eq. (16), while $T_{\max}$ is set respectively to 5000, 10000 and 20000. Note that we obtain different trade-offs between economic cost and number of deaths. In general, by increasing $T_{\max}$, we reduce the economic cost and increase the number of deaths. Evolution of metrics for the case $T_{\max} = 5000$, $H_{\max} = 10000$ is shown in Figure 9 (bottom right plot). In this case, contrarily to the case $T_{\max} = 10000$ and $H_{\max} = 20000$, intensive therapy control exerts the tightest control for a given short period.

At last, Table I reports results for the case $T_{\max} = 10000$, $H_{\max} = 10000$. Observe that the performance of this last case is almost indistinguishable from the case $T_{\max} = 5000$, $H_{\max} = 10000$ (which requires just half of the intensive therapy facilities) both in terms of deaths and economic cost.

In conclusion, in our scenario keeping the ratio $T_{\max}/H_{\max} \approx 2$ appears to be the best choice, as it guarantees that the tightest control is essentially always exerted by hospitalizations in dynamic conditions. Then $T_{\max}$ (and consequently $H_{\max}$) should be chosen instead to achieve the desired trade-off between deaths and economic cost (as previously observed, deaths are more sensitive to parameters than economic costs). In our analysis, we have neglected the costs related to the creation/maintenance of sanitary facilities (which are typically small with respect to general economic costs due to restrictions) to limit the number of free parameters. However, extending the model to include such costs would be relatively immediate.

VI. A COMPARATIVE ANALYSIS WITH OPTIMAL CONTROL

In this section, we perform a comparative analysis of the proposed model against optimal control and homogeneous models to assess its effectiveness and advantages in addressing the research problem.

Table I
COSTS AND DEATHS [$k \equiv 10^3$]

$T_{\max}$	$H_{\max}$	cost ($\alpha = 1$)	cost ($\alpha = 2$)	cost ($\alpha = 3$)	deaths
$5k$	$10k$	$2.03k$	$13.0\ k$	$102\ k$	$13.2\ k$
$10k$	$10k$	$2.03k$	$13.0\ k$	$101\ k$	$13.2\ k$
$10k$	$20k$	$1.94k$	$11.1\ k$	$71.3\ k$	$25.3\ k$
$10k$	$30k$	$1.92k$	$10.9\ k$	$66.6\ k$	$35.9\ k$
$10k$	$50k$	$2.12k$	$14.6\ k$	$115\ k$	$42.2\ k$
$20k$	$40k$	$1.88k$	$10.2\ k$	$59.3\ k$	$49.0\ k$

$T_{\max} = 10000, H_{\max} = 20000$ $T_{\max} = 10000, H_{\max} = 30000$

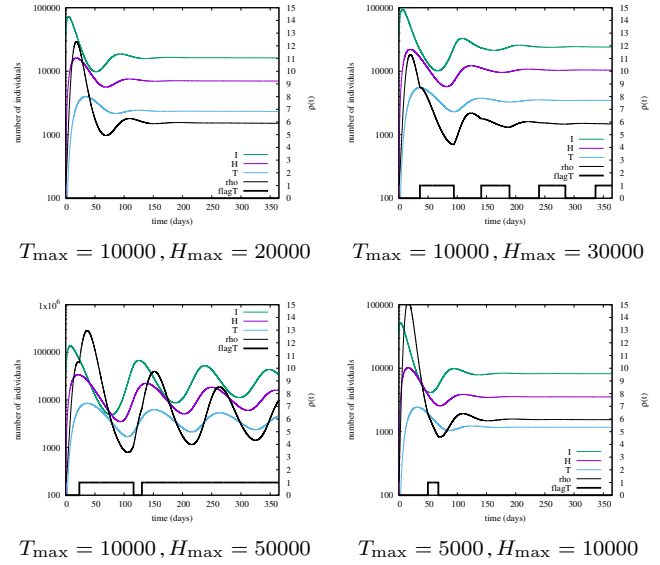$T_{\max} = 10000, H_{\max} = 50000$ $T_{\max} = 5000, H_{\max} = 10000$

Figure 9. Evolution of $I(t)$,$T(t)$ (left y axes) and $\rho(t)$ (right y axes), for different combinations of $T_{\max} = \widehat{T}$ and $H_{\max}$, and fixed $\widehat{H} = 100000$. The rectangles at the bottom of the plots indicate periods in which $\rho(t)$ is determined by $T(t)$.

In this section, we compare the Rate and HT controllers with optimal control during the first phase of the pandemic in which vaccines are still unavailable. All experiments refer to the single-class version of the model in Eq. (1).

In [50], various government intervention strategies are compared against a specific percentage of the deceased population while employing different control policies. We replicate similar experiments and present the numerical solutions obtained via the optimal control approach within a time horizon $t_{\max} = 365$ days. We fix $\kappa_1 = 200$, $\kappa_3 = 20$, and $\zeta = 4$, and we let κ_2 to vary from 10^5 to 10^8.

The considered economic cost corresponds to the teal curve depicted in Figure 3. Such cost has been chosen non-convex, on purpose, to put the Rate control strategy in the most challenging conditions (indeed Proposition 1 and 2 do not hold). Observe that, with our choice of parameters, the first term of the objective function in Eq. (4) is typically small with respect to the third, and therefore the choice of κ_2 becomes fundamental to determine the proper trade-off between economic cost and death/ICU occupancy, where the last two metrics are highly correlated, since by tightly controlling ICU occupancy, we exert tight control on the deaths and vice versa.

As discussed in the Supplemental Material [5], the average sojourn time in state I has been set equal to 8 days and that in states H and T to 16 days. Therefore $\gamma = 1/8$, $\phi = \tau = 1/16$. The transition probabilities between compartments I, H,
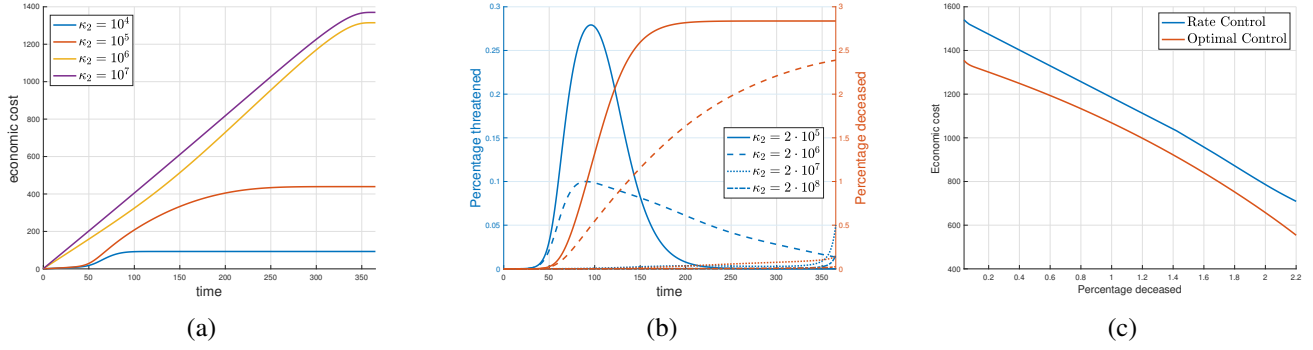
Figure 10. (a) Economic cost and control effort via optimal control (b) Percentage of threatened and deceased individuals via optimal control implementation. (c) Comparison of optimal control and Rate control strategies
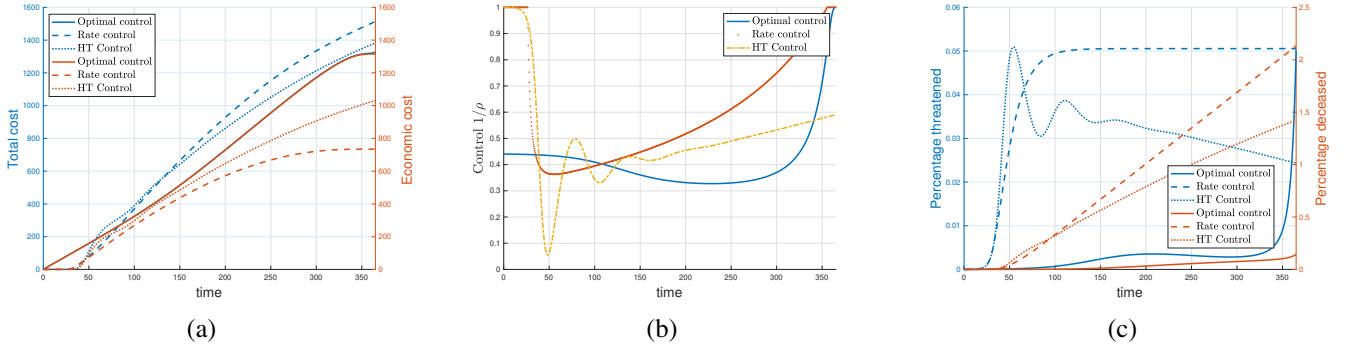

Figure 11. (a) Comparison of different control strategies: (a) Overall costs and economic costs; (b) Control function. (c) Percentage of threatened and deceased individuals.

T, and D, satisfying constraint (2), are set for simplicity as follows: $p^{IH} = p^{HT} = \hat{p}^{TD} = p^{1/3}$ with overall mortality rate $p = 0.01$. The assumed value for the basic reproduction number has been fixed to $\mathcal{R}_0 = 3$, as reported in [51], and the healthcare capacity parameter to $3.33 \cdot 10^{-3}$.

In Figure 10(a), the economic cost (in blue) and the control (in red) are shown as a function of time. For lower values of the parameter ($\kappa_2 \in [10^5, 10^6]$), the control measures are moderate and remain relatively constant for a brief period of approximately 50 days. After this initial phase, the control is tighter, reaching its maximum level of restriction. During this period, stringent measures are implemented to contain the epidemic effectively. Subsequently, as the situation improves or specific goals are achieved, the control is gradually relaxed, allowing for a more lenient approach to managing the epidemic. This sequential pattern of moderate-tightened-relaxed control measures aims to strike a balance between mitigating the spread of the disease and minimizing the socioeconomic impact on the population. The stringent initial intervention effectively disrupts the early exponential growth of the epidemic, leading to a dampened peak number of infections. In both previous cases at the end of the observation window, i.e., for $t \approx t_{\max}$, the population reaches herd immunity. As we increase the value of κ_2, as expected, the control becomes more stringent and is kept constant for most of the time (around 350 days). At the same time, the healthcare system experiences less stress, and the number of deaths decreases at the expense of higher economic costs. Notably, when setting κ_2 above $2 \cdot 10^7$, we

can confidently guarantee that the peak number of patients requiring intensive care remains below around 30000 (see Figure 10(b) where blue curves refer to ICU occupancy and red curves to cumulative deaths). This behavior highlights the importance of appropriately calibrating control parameters to achieve optimal outcomes in managing the epidemic and preventing overwhelming pressure on the healthcare infrastructure. Observe that at the end of the observation window, i.e., for $t \approx t_{\max}$, the control is always completely released, i.e., $\rho(t_{\max}) = 1$. This effect is a by-product of the optimal control approach, which does not account for what happens when $t > t_{\max}$. Indeed, as t approaches $t_{\max}$, releasing the control leads to an instantaneous reduction of the economic cost, while, due to the delay, the resulting increase in ICUs and deaths is negligible (as it will take place after $t_{\max}$).

The analysis in Figure 10(c) highlights the trade-offs between economic cost and human lives achieved by optimal control and Rate control, respectively. The curves have been obtained by varying parameter $\kappa_2 \in [10^5, 10^8]$ for optimal control, $\lambda \in [1000, 700000]$ for Rate control. We have disregarded the healthcare stress cost, using the total number of deaths as a proxy of it. It should be noted that the optimal control strategy proves to be the most effective, outperforming the rate control strategy. However, if we fix the number of deaths, for example, to 0.2% (i.e., 100000 deaths), the rate control strategy exhibits only a slightly worse economic cost. The difference between the economic cost curves of the two strategies is not substantial, with a modest 7% increase

obtained by the rate control strategy. Despite the increase in economic costs resulting from the rate control strategy, the difference is relatively small, indicating that both strategies remain competitive in managing the epidemic.

It is worth remarking that approximately the same value of the overall objective function in Eq. (4), which takes into account economic cost, deaths, and healthcare stress in the optimal control strategy, can be achieved through fairly different approaches. Figure 11 provides a comparison among the optimal control strategy with $\kappa_2 = 2 \cdot 10^7$, the Rate control with $\lambda = 120000$, and the linear HT control with $\rho_H(H) = \min\left(15, \frac{H_0}{H_0 - H}\right)$ and $\rho_T(T) = \min\left(15, \frac{T_0}{T_0 - T}\right)$, with and $H_0 = 480000$ and $T_0 = 300000$. While the overall cost for the three strategies is approximately the same, the different components of the cost are significantly different. For what concerns the economic cost, the optimal control strategy appears to be the least favorable, resulting in the highest economic burden compared to the other strategies (the economic cost for the optimal control strategy is hardly distinguishable from the overall cost). On the other hand, the rate control strategy is the most efficient in minimizing economic costs, offering a more economically sustainable approach. The HT control strategy falls in an intermediate position, achieving a balance between cost-effectiveness and epidemic management. Regarding the number of deaths, the optimal control strategy demonstrates its strength, resulting in the lowest fatality rate among the three strategies. It effectively minimizes the loss of life during the epidemic. Conversely, the rate control strategy shows the highest number of deaths, indicating that this approach is less effective in preventing fatalities. The HT control strategy lies in between, offering an intermediate level of protection against the loss of life compared to the other two strategies. In conclusion, adopting the overall cost as the unique driver for the choice of $\rho(t)$ turns out to be not particularly appealing to decision-makers because it does not allow them to exert direct control on the different components of the cost.

VII. EXPERIMENTS IN A COMPREHENSIVE SCENARIO

Our numerical results are obtained in a reference scenario roughly inspired by the actual evolution of COVID-19 in Italy during a period of 3 years, starting from the onset of the virus at the beginning of 2020. During this period, the dynamics of COVID-19 in Italy (and similarly in other European countries) have been characterized by three main phases, each spanning about one year:

1) **first phase**: in this phase the most dangerous strains of the virus, e.g., the alpha and delta mutations, propagated in the absence of pharmaceutical interventions (vaccines), causing the majority of all deaths attributed to COVID-19.
2) **second phase**: since the beginning of 2021, vaccines started to be massively distributed to the population, and almost all individuals (excluding no-vax people) completed the vaccination cycle (by receiving one or two doses) by the end of the second year.
3) **third phase**: since the beginning of 2022, with the onset of the omicron variant, less dangerous but more virulent

strains became prevalent, substituting the initial strains. Vaccines originally developed for the alpha and delta mutations also protected people against the omicron variant, though with reduced efficacy.

To capture the above dynamics, we made some simplifying approximations to limit the model complexity: we assume that a single variant (strain 1), with basic reproduction number $R_0^1 = 6$, propagates during the first 2 phases, after which a new variant (strain 2) appears with higher $R_0^2 = 12$ and reduced mortality (by factor q_{21} with respect to the mortality of strain 1, for each class of people).

The parameters of our reference scenario are summarized in Table IV of the Supplemental Material [5]. Although our model and parameters can only roughly describe the actual dynamics of COVID-19 in Italy, they provide a realistic scenario in which different virus mitigation strategies can be compared, offering valuable insights. Of course, in our model for the reference scenario, we stratify the population using the $f_{r,p}$ distribution computed for Italy, as explained in [5]. Transition probabilities between compartments I,H,T,D satisfying constraint (2) are set for simplicity as follows: $p_{r,p}^{IH} = p_{r,p}^{HT} = \hat{p}_{r,p}^{TD} = p^{1/3}$.

Strain 1 starts at time 0 with 1 initially infected individual. Similarly, strain 2 starts at time t_2 with 1 initially infected individual. We consider the economic cost function: $\mathfrak{C}(\rho) = (\rho - 1)^\alpha$ which satisfies the assumptions of Proposition 1 for $\alpha \geq 1$, and allows us to explore the impact of costs caused by more substantial non-pharmaceutical interventions by varying the single parameter α. We emphasize that the resulting scenario is not specific to Italy: similar assumptions and parameters could describe equally well, at a high level, the dynamics of COVID-19 in other mid-size European countries or a single US state with a comparable population size. At last, while each of the first two phases lasted approximately one year, in our analysis to have a complete view of the potential impact of different control approaches, we have also considered cases in which no effective treatments have been available for several years. When the epidemic spread out at the beginning of 2020, and the first decisions had to be made, no one could predict how long it would have taken to have effective vaccines/treatments available. In the following, for the sake of simplicity, we neglect the term associated with the healthcare system stress by taking into consideration only social (deaths) and economic costs, this corresponds to set $\kappa_2 = 0$.

In the following two subsections we first examine the interplay between mobility restrictions, enforced through our two Rate and HT controls, and vaccination prioritization schemes (MSF and MVF) hence considering the first two years of our reference scenario. Then, we consider the complete three-years comprehensive scenario.

A. Mobility restrictions and vaccinations

We first consider the 'first' and 'second phase' of our reference scenario, considering the joint impact of vaccination policies and control strategies during the first two years of the pandemic. Recall from Sec. III-B that we focus on two

extreme vaccine prioritization policies: Most Vulnerable First (MVF) and Most Social First (MSF).

We will consider a single type of vaccine to be administered in two doses separated by a variable interval of Δ days. In this way, we can address an issue raised in some countries, e.g., the UK, when vaccines started to be available for mass distribution, i.e., whether it is better to follow the recommended protocol ($\Delta = 21$ days) or to give one dose to the largest possible population, before administering the second dose. The latter policy, which aims at partially immunizing a vast portion of the population, corresponds to choosing $\Delta = 135$ days. In our investigation, we assume the vaccination rate to be constant and such that the entire population can receive two doses after 9 months (270 days).

No vaccine is available during the first year (first phase). To better compare our two control strategies, we initially start the system at the equilibrium point (I^*, H^*, T^*), disregarding the transient needed to reach such equilibrium.[3] Under the HT strategy, we assume that control is always determined by the occupation of regular hospitals, rather than ICU, by adequately setting the ratio $T_{\max}/H_{\max}$. Moreover, note that the parameters of the HT strategy can be tuned to achieve the desired number I^* of infected people at the beginning of the pandemic. This allows us to compare the trade-offs achievable by our two control policies.

Given the current understanding of COVID-19 vaccines, one limitation of the approach is the uncertainty surrounding the specific efficacy of different vaccines and their effectiveness against emerging variants. Vaccine efficacy can vary depending on age, underlying health conditions, and individual immune response. Additionally, the duration of vaccine-induced protection and the potential for waning immunity over time are still being studied. As a result, the parameters related to vaccine prioritization, such as the efficacy rates and the duration of protection, are subject to a range of values rather than precise estimates. The lack of comprehensive knowledge about these parameters restricts the ability to determine an optimal vaccination strategy with certainty. Therefore, the study may need to consider a range of plausible values for vaccine-related parameters and perform sensitivity analyses to assess the robustness of the results under different scenarios. Given the considerations above, we introduce variability in the efficacy ratio between the first and second doses of the vaccine. Specifically, we examine two different values for this ratio, denoted as $\mathsf{VE}^1/\mathsf{VE}^2$, namely 0.3 and 0.6. Meanwhile, we keep the efficacy of the second dose fixed at $\mathsf{VE}^2 = 0.9$. By incorporating this range of values for the efficacy ratio, we account for the uncertainty surrounding the relative effectiveness of the two vaccine doses.

The achievable trade-offs between economic cost and number of deaths, measured at the end of the second year, are shown in plots (a),(b),(c), and (d) of Fig. 12, for the four combinations arising from the two considered control policies and the two considered efficacy ratios (see plot titles). Each plot contains four curves related to the four combinations of

vaccination policies (MSF vs. MVF, $\Delta = 21$ vs. $\Delta = 135$).

Several observations are in order. First, the MSF policy (green and blue curves) generally outperforms MVF (red and purple curves). This fact is not trivial and depends crucially on the extent of the negative correlation between r and p in the population distribution $f_{r,p}$. Note that the MSF policy is hardly implementable in practice. Indeed, only the MVF policy has been deployed in many countries, by simple age prioritization, except for special categories of workers (e.g., healthcare workers) who have also received the vaccine in advance due to their exposition to the virus.

Second, as expected, the efficacy ratio of 0.6 leads to better outcomes than the efficacy ratio of 0.3. In particular, delaying the distribution of the second dose ($\Delta = 135$) is not advisable if the first dose is relatively ineffective (efficacy ratio 0.3).

Third, the impact of different control strategies is fairly small, with rate control slightly outperforming HT control. The best possible trade-offs, i.e., the lowest possible curves, are generated by the rate control, MSF, and a properly tuned Δ (note the crossing between blue and green curves on plot Fig. 12(c)).

The effect of the two control strategies, combined with different vaccination policies, can be better understood by looking at temporal dynamics shown in Fig. 13 for rate and HT control. In both cases, we assume an initial number of infected people $I^* = 32,000$ (corresponding to $\lambda_C = 4,000$) while restricting ourselves to an efficacy ratio of 0.6.

The evolution of $D(t)$, $I(t)$, $T(t)$, $\rho(t)$ in Fig. 13 is shown by curves of different colors, respectively red, green, blue, and black. Thick (thin) lines correspond to MVF (MSF). Solid (dashed) lines correspond to $\Delta = 21$ ($\Delta = 135$). Let us start with the simpler case of rate control in Fig. 13. Here, $I(t)$ is maintained constant through the entire period of two years. When vaccinations start (day 365), two extreme behavior for $\rho(t)$ arise, as expected, by MSF with $\Delta = 21$ (thin dashed black line) and MVF with $\Delta = 21$ (thick dashed black line), with the other curves (related to $\Delta = 135$) lying in between these two. MSF with $\Delta = 21$ allows us to release social restrictions more quickly, lowering the economic cost at the expense of more deaths. The case of HT control in Fig. 13 is more complex, since here $I(t)$ is not constant and, in fact, decreases drastically during the second year thanks to the self-adaptive nature of HT control.

The fact that better trade-offs are achieved by the not self-adaptive rate control at the end of the second year may appear counter-intuitive. Note, however, that such better trade-offs are only possible under a carefully tuned MSF policy, and they are thus hardly achievable in practice. At last, observe that in a more realistic setting, one might not arbitrarily choose the rate of new infections. For example, if one cannot operate below $\lambda_C = 4,000$, from Fig. 13, the best option would likely be MVF, which produces significantly fewer deaths at the expense of a tolerable and largely justifiable increase of the economic cost. Interestingly, in this case, $\Delta = 135$ would produce a significantly lower penalty in the economic cost with respect to $\Delta = 21$ while generating an almost identical number of deaths.

---

[3]A comprehensive analysis of the complete scenario also comprising the initial transient will be presented later in Sec. VII-B.
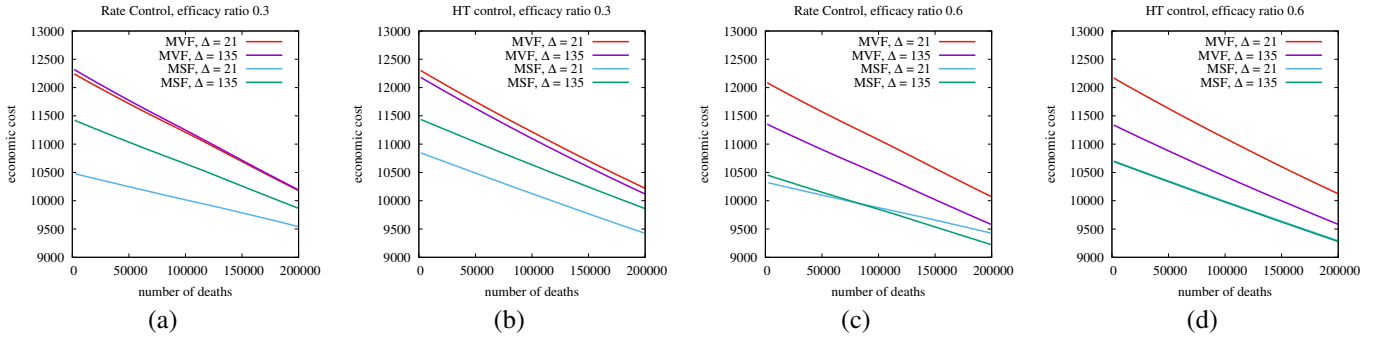
Figure 12. Impact of vaccination policies and control strategies on deaths and economic cost. All individuals are vaccinated in 270 days.
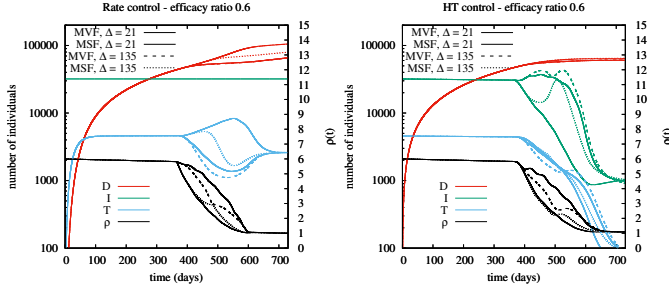

Figure 13. Evolution of $I(t), D(t), T(t), \rho(t)$ in the case of Rate control (left) and HT control (right), efficacy ratio 0.6, and different vaccination policies (different line styles of the same colour).

B. Control in a comprehensive scenario

At last, we consider a scenario encompassing all three epidemic phases, spanning over three years, as described in sec. VII. The MVF-$\Delta = 21$ vaccination policy was chosen in light of the fact that many countries have largely adopted this policy. The ratio between the first and second doses' efficacy has been set to 0.6.

Figure 14(a) and Figure 14(b) report the evolution of the metrics, respectively, for the case in which the control is on the rate of new infected ($\lambda_C = 4,000$) and the HT (with $T_{\max} = 20000$ and $H_{\max} = 40000$). Parameters have been set so that the two controls operate around approximately the same operational point during the first year.

Rate control appears more reactive in the early phase of the epidemic. As already observed, due to its intrinsic delay in the control ring, HT control exhibits some initial oscillations, which are not observable when rate control is applied. Therefore, it should not be surprising that rate control leads to better performance indices at the end of the first year, as shown in Table II. Note that costs are expressed in arbitrary units, while deaths are expressed in thousands. However, when the second variant starts spreading, the rate-control strategy may overreact, forcing the system to work in over-restricted conditions for quite a long time (note that at the end of the three-year period, rate-control is far from being completely relieved). Instead, HT control can automatically adjust its operational point as an effect of the mutated environmental conditions, i.e., a smaller intrinsic lethality index of the variant and a significant fraction of vaccinated individuals who are protected against severe outcomes.

We remark that these strategies, which tightly and precisely control either the infection rate or the hospitalization/ICU occupancy, are hardly implementable. However, they provide valuable insights. To shed light on more practical controls, we examine an implementable rough version of the HT control, denoted as Imperfect HT (IHT). Figure 14(c) shows the evolution of the epidemic when the IHT strategy is adopted. In this case, the control dynamically selects the current alert level from the following finite set *green, white, yellow, orange, red, purple*. A different set of non-pharmaceutical restrictions corresponds to every alert level, determining a corresponding value of $\rho(t) \in \{1, 2, 3, 5, 12, 15\}$ (note that intermediate values of $\rho(t)$ corresponding to different alert levels, do not need to be perfectly known). Every week a simple threshold mechanism is implemented to establish the current alert level for the following week, with normalized thresholds (with respect to $H_{\max}$ or $T_{\max}$) set respectively to $\{0.01, 0.1, 0.2, 0.4, 1.0\}$. Any alert level must be maintained for at least three weeks before it can be decreased. Despite the behavior of IHT does not significantly deviate from HT, a high extra economic cost is paid for the effect of unavoidable oscillations between consecutive alert levels, especially for large values of α.

VIII. CONCLUSIONS

Our research draws on lessons learned from the COVID-19 pandemic. It takes a comprehensive approach to addressing the challenges of effectively planning and implementing interventions in large communities, such as those the size of a country. The overarching goal is to strike a balance between minimizing economic costs and reducing fatalities, a critical endeavor in pandemic management.

At the heart of our study lies a sophisticated multi-class model. This model is designed to account for the complex relationship between mortality rates and variations in risk exposure among different population segments. It also accounts for the intriguing negative correlation that often exists between

Table II
COMPARISON OF CONTROL STRATEGIES IN A COMPREHENSIVE
SCENARIO: ECOMOMIC COSTS AND DEATHS

	1st year				three years			
	Cost			Deaths	Cost			Deaths
α	1	2	3		1	2	3	
rate	1.68	8.18	39.9	41.1	3.35	13.5	58.0	70.5
HT	1.76	9.22	50.2	45.8	3.19	13.4	64.6	78.8
IHT	2.02	15.5	146	40.6	3.71	22.1	187	68.7

(a) Rate Control, $\lambda_C = 4000$.

(b) HT control: $T_{\max} = \widehat{T} = 20000$; $H_{\max} = 40000$, $\widehat{H} = 100000$.
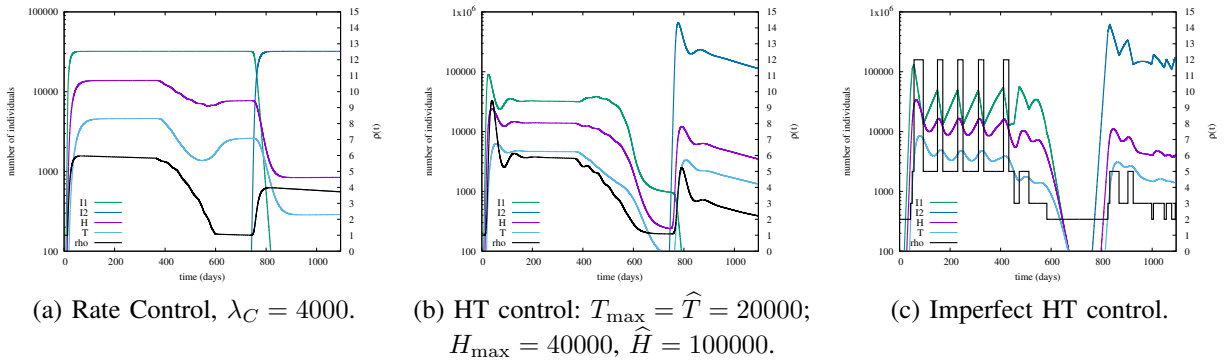
(c) Imperfect HT control.

Figure 14. Evolution of $I(t)$, $H(t)$, $T(t)$ (left y axes) and $\rho(t)$ (right y axes) in the comprehensive scenario.

an individual's age and their level of risk exposure to the virus. Importantly, this correlation is not uniform across countries, and our model is pioneering in its ability to incorporate this variation trough a data-driven approach. By doing so, our model provides a more realistic and holistic representation of epidemic evolution that accounts for these intricate dynamics.

Through our analysis, we have uncovered a critical aspect of epidemic control. We have found that strategies employed to control outbreaks, whether based on monitoring infection rates or assessing the burden on the healthcare system, can be subject to significant instability. This instability is particularly evident when we move from idealized scenarios to the complexity of the real world, characterized by uncertainty and influenced by various parameters not always readily accessible.

It is important to underline that there is no one-size-fits-all approach when it comes to epidemic control. What is appropriate and effective depends on the specific context, goals, and resources available. Our research recognizes this and does not claim to offer a universally superior solution. Instead, it takes a pragmatic perspective. We prioritize simplicity and ease of implementation, recognizing the practical challenges that decision-makers often face. Our goal is to provide a toolkit of strategies that can be considered alongside more complex models and provide policy-makers with a range of options.

Consistent with real-world responses to the COVID-19 pandemic, our research provides insights into the practical effectiveness of rate control and hospitalization strategies. We also conduct a comparative analysis of vaccination policies, looking at different approaches and variations in dosing intervals, inspired by the experiences of countries such as the United Kingdom and Italy. This comparative approach allows us to explore the potential impact of different vaccination strategies in different epidemiological contexts, providing valuable guidance to policy-makers.

In summary, our research aims to provide a comprehensive, data-driven, and practical approach to epidemic control. It recognizes the complexities and challenges faced in real-world, country-sized communities and aims to bridge the gap between theoretical modeling and actual policy implementation, ultimately contributing to more effective and realistic strategies for managing pandemics.

REFERENCES

[1] R. M. Anderson, H. Heesterbeek, D. Klinkenberg, and T. D. Hollingsworth, "How will country-based mitigation measures influence the course of the COVID-19 epidemic?" *Lancet*, vol. 395, no. 10228, pp. 931–934, 2020.

[2] M. Kantner and T. Kopruki, "Beyond just flattening the curve: Optimal control of epidemics with purely non-pharmaceutical interventions," *Journal of Mathematics in Industry*, vol. 10, p. 23, 08 2020.

[3] F. Fallucchi, M. Faravelli, and S. Quercia, "Fair allocation of scarce medical resources in the time of covid-19: What do people think?" *Journal of Medical Ethics*, vol. 47, no. 1, pp. 3–6, Jan. 2021.

[4] W. O. Kermack and A. G. McKendrick, "A contribution to the mathematical theory of epidemics," *Proceedings of the Royal Society of London. Series A, Containing Papers of a Mathematical and Physical Character*, vol. 115, no. 772, pp. 700–721, Aug. 1927.

[5] F. Galante, C. Ravazzi, M. Garetto, and E. Leonardi, "Supplemental material – planning interventions in a controlled pandemic: the covid-19 case," *submitted to IEEE Transactions on Network Science and Engineering*, 2023.

[6] D. Mistry et al., "Inferring high-resolution human mixing patterns for disease modeling," *Nature Communications*, vol. 12, 01 2021.

[7] P. E. Paré, C. L. Beck, and T. Basar, "Modeling, estimation, and analysis of epidemics over networks: An overview," *Annual Reviews in Control*, vol. 50, pp. 345–360, 2020.

[8] H. M. Taylor, "Some models in epidemic control," *Mathematical Biosciences*, vol. 3, pp. 383–398, 1968.

[9] A. Abakuks, "An optimal isolation policy for an epidemic," *Journal of Applied Probability*, vol. 10, no. 2, pp. 247–262, 1973.

[10] R. Morton and K. H. Wickwire, "On the optimal control of a deterministic epidemic," *Advances in Applied Probability*, vol. 6, no. 4, pp. 622–635, 1974.

[11] K. Wickwire, "Optimal isolation policies for deterministic and stochastic epidemics," *Mathematical Biosciences*, vol. 26(3) pp. 325–346, 1975.

[12] S. P. Sethi and P. W. Staats, "Optimal control of some simple deterministic epidemic models," *The Journal of the Operational Research Society*, vol. 29, no. 2, pp. 129–136, February 1978.

[13] E. Hansen and T. Day, "Optimal control of epidemics with limited resources," *Journal of Mathematical Biology*, vol. 62, pp. 423–451, 2011.

[14] T. Kruse and P. Strack, "Optimal Control of an Epidemic through Social Distancing," Cowles Foundation for Research in Economics, Yale University, Cowles Foundation Discussion Papers 2229, Apr. 2020.

[15] H. Behncke, "Optimal control of deterministic epidemics," *Optimal Control Applications and Methods*, vol. 21, pp. 269 – 285, 11 2000.

[16] L. Bolzoni, E. Bonacini, C. Soresina, and M. Groppi, "Time-optimal control strategies in sir epidemic models," *Mathematical Biosciences*, vol. 292, pp. 86–96, 2017.

[17] J. R. Birge, O. Candogan, and Y. Feng, "Controlling epidemic spread: Reducing economic losses with targeted closures," *Management Science*, vol. 68, no. 5, pp. 3175–3195, 2022.

[18] T. Britton, M. Deijfen, and A. N. Lagerås, "Optimal control of vaccination dynamics during an influenza epidemic," *Journal of Mathematical Biology*, vol. 78, no. 1-2, pp. 135–160, 2019.

[19] Z. Feng and X.-Q. Zhao, "Optimal vaccination and treatment in a multi-group epidemic model," *Journal of Mathematical Biology*, vol. 67, no. 6–7, pp. 1549–1576, 2013.

[20] J. Zhang, M. Li, and Z. Ma, "Optimal control of a vaccination model with vaccination age," *Mathematical Biosciences and Engineering*, vol. 11, no. 5, pp. 1055–1076, 2014.

[21] F. Altarelli, "Containing epidemic outbreaks by message-passing techniques," *Physical Review X*, vol. 4, p. 021024, 2014.

[22] A. Galeotti, B. Golub, and S. Goyal, "Strategic immunization and group structure," *American Economic Journal: Microeconomics*, vol. 5, no. 2, pp. 1–32, 2013.

[23] L. Matrajt, J. Eaton, T. Leung, and E. R. Brown, "Vaccine optimization for covid-19: Who to vaccinate first?" *Science Advances*, vol. 7, no. 6, 2021.

[24] C. M. Saad-Roy et al., " Epidemiological and evolutionary considerations of SARS-CoV-2 vaccine dosing regimes," *Science*, vol. 372, no. 6540, pp. 363–370, 2021.

[25] J. R. Goldstein, T. Cassidy, and K. W. Wachter, "Vaccinating the oldest against COVID-19 saves both the most lives and most years of life," *PNAS*, vol. 118, no. 11, 2021.

[26] J. Medlock and A. P. Galvani, "Optimizing Influenza Vaccine Distribution," *Science*, vol. 325, no. 5948, pp. 1705–1708, 2009.

[27] F. G. Sandmann, N. G. Davies, A. Vassall, W. J. Edmunds, M. Jit, and Centre for the Mathematical Modelling of Infectious Diseases COVID-19 working group, "The potential health and economic value of SARS-CoV-2 vaccination alongside physical distancing in the UK: a transmission model-based future scenario analysis and economic evaluation," *The Lancet Infectious Diseases*, vol. 21, no. 7, pp. 962–974, 2021.

[28] M. Monod et al., "Age groups that sustain resurging covid-19 epidemics in the united states," *Science*, vol. 371, no. 6536, 2021.

[29] P. Jentsch, M. Anand, and C. T. Bauch, "Prioritising COVID-19 vaccination in changing social and epidemiological landscapes: a mathematical modelling study," *The Lancet Infectious Deseases*, vol. 21, pp. 1097–1106, 2021.

[30] L. Freddi, "Optimal control of the transmission rate in compartmental epidemics," *Mathematical Control & Related Fields*, vol. 12, no. 1, pp. 201–223, 2022.

[31] G. Kaplan, B. Moll, and G. L. Violante, "The great lockdown and the big stimulus: Tracing the pandemic possibility frontier for the u.s." National Bureau of Economic Research, Working Paper 27794, September 2020.

[32] L. Cianfanelli, F. Parise, D. Acemoglu, G. Como, and A. Ozdaglar, "Lockdown interventions in sir models: Is the reproduction number the right control variable?" in *CDC*, 2021, pp. 4254–4259.

[33] R. Carmona and P. Wang, "Finite state mean field games with major and minor players," 2016.

[34] A. Aurell, R. Carmona, G. Dayanikli, and M. Laurière, "Optimal incentives to mitigate epidemics: A stackelberg mean field game approach," *SIAM Journal on Control and Optimization*, vol. 60, no. 2, pp. S294–S322, 2022.

[35] R. Elie, E. Hubert, and G. Turinici, "Contact rate epidemic control of COVID-19: an equilibrium view," *Mathematical Modelling of Natural Phenomena*, vol. 15, p. 35, Jun. 2020.

[36] T. Britton, F. Ball, and P. Trapman, "A mathematical model reveals the influence of population heterogeneity on herd immunity to sars-cov-2," *Science*, vol. 369, no. 6505, pp. 846–849, 2019.

[37] D. Acemoglu, V. Chernozhukov, I. Werning, and M. D. Whinston, "Optimal targeted lockdowns in a multi-group sir model," National Bureau of Economic Research, Tech. Rep. 27102, 2020.

[38] R. Bhattacharyya, S. Mukherjee, and A. Mukhopadhyay, "Modelling the covid-19 pandemic in india: A compartmental model study considering heterogeneity and mobility," *Chaos, Solitons & Fractals*, vol. 146, p. 110922, 2021.

[39] R. Chowdhury et al., "Dynamic interventions to control covid-19 pandemic: A multivariate prediction modelling study comparing 16 worldwide countries," *European Journal of Epidemiology*, vol. 35, no. 5, pp. 389–399, 2020.

[40] X. Li, M. Liu, Y. Deng, Z. Sun, L. Xiao, and Y. Feng, "Epidemiological and dynamical analysis of covid-19 transmission in shenzhen china," *Annals of Translational Medicine*, vol. 8, no. 21, p. 1377, 2020.

[41] A. Charpentier, R. Elie, M. Laurière, and V. C. Tran, "COVID-19 pandemic control: balancing detection policy and lockdown intervention under ICU sustainability," 2020.

[42] C. Signorelli and A. Odone, "Age-specific COVID-19 case-fatality rate: no evidence of changes over time," *International Journal of Public Health*, vol. 65, no. 8, pp. 1435–1436, Sep. 2020.

[43] R. Pastor-Satorras, C. Castellano, P. Van Mieghem, and A. Vespignani, "Epidemic processes in complex networks," *Reviews of Modern Physics*, vol. 87, no. 3, pp. 925–979, 2015.

[44] M. E. Newman, "Spread of epidemic disease on networks," *Physical Review E*, vol. 66, no. 1, p. 016128, 2002.

[45] M. J. Keeling and K. T. D. Eames, "Networks and epidemic models," *Journal of The Royal Society Interface*, vol. 2, no. 4, pp. 295–307, 2005.

[46] X.-J. Li, C. Li, and X. Li, "Minimizing social cost of vaccinating network sis epidemics," *IEEE Transactions on Network Science and Engineering*, vol. 5, no. 4, pp. 326–335, 2018.

[47] L. Matrajt, T. Britton, M. E. Halloran, and I. M. Longini, "One versus two doses: What is the best use of vaccine in an influenza pandemic?" *Epidemics*, vol. 13, pp. 17–27, 2015.

[48] M. Xia, L. Böttcher, and T. Chou, "Controlling Epidemics Through Optimal Allocation of Test Kits and Vaccine Doses Across Networks," *IEEE Transactions on Network Science and Engineering*, vol. 9, no. 3, pp. 1422–1436, 2022.

[49] A. R. Hota, J. Godbole, and P. E. Paré, "A Closed-loop Framework for Inference, Prediction, and Control of SIR Epidemics on Networks," *IEEE Transactions on Network Science and Engineering*, vol. 8, no. 3, pp. 2262–2278, 2021.

[50] A. Kasis, S. Timotheou, N. Monshizadeh, and M. Polycarpou, "Optimal intervention strategies to mitigate the covid-19 pandemic effects," *Scientific Reports*, vol. 12, no. 1, p. 6124, 2022.

[51] J. Yuan, M. Li, G. Lv, and Z.-K. Lu, "Monitoring transmissibility and mortality of covid-19 in europe," *International Journal of Infectious Diseases*, vol. 95, pp. 311–315, 2020.

Franco Galante received the Bachelor Degree from Università degli Studi di Padova in 2018, and the Master Degree from Politecnico di Torino in Communications and Computer Network Engineering in 2020. In 2019 he spent a semester at TU Delft. He is currently a Ph.D. student at Politecnico di Torino within the department of Electronics and Telecommunications. His research interests include dynamics over networks, randomized algorithms and control of networks.

Chiara Ravazzi (M'13) is currently a Senior Researcher with the CNR-IEIIT and Adjunct Professor at Politecnico di Torino. She received the Ph.D. degree in Mathematics for Engineering Sciences from Politecnico di Torino, in 2011. In 2010, she was a visiting member at the Massachusetts Institute of Technology, Cambridge (LIDS) and, she held Postdoctoral positions with Politecnico di Torino (2011-2016). she served as an Associate Editor for IEEE Transactions on Signal Processing from 2019 to 2023, and she currently holds the same position for IEEE Control Systems Letters (since 2021) and the European Journal of Control (since 2023). Her research interests include learning, optimization and control over networks.

Michele Garetto (M'04) received the Dr.Ing. degree in Telecommunication Engineering and the Ph.D. degree in Electronic and Telecommunication Engineering, both from Politecnico di Torino, Italy, in 2000 and 2004, respectively. In 2002, he was a visiting scholar with the Networks Group of the University of Massachusetts, Amherst, and in 2004 he held a postdoctoral position at the ECE department of Rice University, Houston. He is currently associate professor at the Computer Science Department of University of Torino, Italy.

Emilio Leonardi is a professor with the Department of Electronics and Telecommunications, Politecnico di Torino. He visited: UCLA, CS dept. in 1995, Lucent Bell-labs (Holmdel) in 1999, Stanford EE dept. in 2001, Sprint Labs (Burlingame) in 2003, NEC Labs (Heidelberg) in 2012, INRIA (Sophia Antipolis) in 2016. His research interests include performance evaluation of computer networks and distributed systems, dynamics over networks, and human centric computation.